

1 **400 years of summer hydroclimate from stable isotopes in Iberian trees**

2

3 Laia Andreu-Hayles^{1,2}, Caroline C. Ummenhofer^{3,*}, Mariano Barriendos^{4,2}, Gerhard H.

4 Schleser^{5,6}, Gerhard Helle⁵, Markus Leuenberger⁷, Emilia Gutiérrez⁸ and Edward R. Cook¹

5

6 1. Tree-Ring Laboratory, Lamont-Doherty Earth Observatory of Columbia University,
7 Palisades, NY, USA.

8 2. Institut Català de Ciències del Clima (IC3), Barcelona, Catalonia, Spain.

9 3. Department of Physical Oceanography, Woods Hole Oceanographic Institution,
10 Woods Hole, MA, USA.

11 4. Department of Modern History, University of Barcelona, Spain.

12 5. Climate Dynamics and Landscape Evolution, German Centre for Geosciences,
13 Potsdam, Germany.

14 6. Research Center Juelich, Institute of Bio-and Geosciences, Agrosphere (IBG-3);
15 Juelich, Germany.

16 7. Climate and Environmental Physics, University of Bern, Switzerland.

17 8. Department of Ecology, University of Barcelona, Spain.

18

19 *Corresponding authors: Laia Andreu-Hayles <lah@ldeo.columbia.edu>, Tree-Ring

20 Laboratory, Lamont-Doherty Earth Observatory of Columbia University, 61 Route 9W,

21 Palisades, NY 10964, USA; Caroline C. Ummenhofer <cummenhofer@whoi.edu>,

22 Department of Physical Oceanography, Woods Hole Oceanographic Institution, Woods

23 Hole, MA, USA;

24 **Abstract**

25 Tree rings are natural archives that annually record distinct types of past climate variability
26 depending on the parameters measured. Here, we use ring-width and stable isotopes in cellulose
27 of trees from the northwestern Iberian Peninsula (IP) to understand regional summer
28 hydroclimate over the last 400 years and the associated atmospheric patterns. Spatial correlations
29 between tree rings and gridded climate products demonstrate that isotope signatures in the
30 targeted Iberian pine forests are very sensitive to water availability during the summer period,
31 and are mainly controlled by stomatal conductance. Non-linear methods based on extreme events
32 analysis allow for capturing distinct seasonal climatic variability recorded by tree-ring
33 parameters and asymmetric signals of the associated atmospheric features. Moreover, years with
34 extreme high (low) values in the tree-ring records were characterised by coherent large-scale
35 atmospheric circulation patterns with reduced (enhanced) moisture transport onto the
36 northwestern IP. These analyses of extremes revealed that high/low proxy values do not
37 necessarily correspond to mirror images in the atmospheric anomaly patterns, suggesting
38 different drivers of these patterns and the corresponding signature recorded in the proxies.
39 Regional hydroclimate features across the broader IP and western Europe during extreme
40 wet/dry summers detected by the northwestern IP trees compare favourably to an independent
41 multicentury sea level pressure and drought reconstruction for Europe. These independent
42 sources of past climate validate our findings that attribute non-linear moisture signals recorded
43 by extreme tree-ring values to distinct large-scale atmospheric patterns and allow for 400-yr
44 reconstructions of the frequency of occurrence of extreme conditions in summer hydroclimate.

45

46 *Keywords:* tree rings, extreme analyses, atmospheric circulation, hydroclimate, Sea Level

47 Pressure (SLP), Old World Drought Atlas (OWDA), Iberian Peninsula

48

49 **1 Introduction**

50 Located at the westernmost edge of the Mediterranean, the Iberian Peninsula (IP) is exposed to
51 atmospheric phenomena of Mediterranean and North Atlantic origin. Iberian hydroclimate is
52 characterised by strong spatiotemporal variability (Fig. 1). While some eastern and southern
53 Iberian regions are semi-arid, precipitation along the northern coast exceeds 1500 mm/yr with
54 dry summers and wet cool seasons. Despite this, drought is a familiar occurrence in the IP:
55 analysing drought evolution during 1910-2000, Vicente-Serrano (2006) found intense and
56 widespread drought episodes in the 1940s, 1950s, 1980s, and 1990s, with higher intensity in
57 the central and western IP than in the northeastern region. Developing technical solutions to
58 recurring and extended water scarcity through infrastructure building, advanced water
59 management, and legislation has a rich and successful history over past centuries in Spain,
60 which is still reflected today in more dams per capita than in any other country in the world
61 (Llamas 2003). This is even more crucial considering the projected subtropical drying in a
62 warming world due to increased subsidence across the region driven by an expansion of the
63 Hadley cell (Lu et al. 2007; Previdi and Liepert 2007; Lu et al. 2009; Cai et al. 2012;
64 Karnauskas and Ummenhofer 2014; Lau and Kim 2015), which is likely to put further strain
65 on limited water resources in the future. The Mediterranean region has been identified as one
66 of the top climate change hot-spots worldwide (Giorgi 2006). Recent changes in IP
67 precipitation and temperature suggest that some of these trends towards increasing aridity are
68 already under way (Giorgi and Lionello 2008; De Luis et al. 2009; Hoerling et al. 2012).
69 More frequent extremes in hydroclimate, such as floods and droughts, are likely in a warming
70 world (Wentz et al. 2007; Trenberth 2011; Hartmann et al. 2013). Records of past hydroclimate
71 variability thus provide an important long-term context for devising management strategies for

72 water resources. Tree rings are natural archives that can provide information about the Earth's
73 past environmental conditions with precise annual resolution. By applying dendrochronological
74 techniques, it is possible to assess the relationships between trees and environmental factors and
75 use this information to estimate climatic conditions before the existence of instrumental records:
76 i.e., generate palaeoclimatic reconstructions. The traditional tree-ring parameters are annual ring-
77 width (TRW) and maximum density (Fritts 1976), but annually resolved isotopic chronologies
78 based on tree-rings have increased in number during the last few decades (e.g., McCarroll and
79 Loader 2004; Seftigen et al. 2011; Gagen et al. 2012; Loader et al. 2013; Konter et al. 2014;
80 Labuhn et al. 2014; Naulier et al. 2015; and references therein). European multi-proxy
81 precipitation reconstructions over the last 500 years show distinct spatial, seasonal and temporal
82 patterns, especially between central Europe and the IP, including unstable relationships between
83 regional precipitation and large-scale atmospheric patterns (Cook et al. 2002; Pauling et al. 2006;
84 Vicente-Serrano and López-Moreno 2008). Although drought reconstructions covering Europe
85 (Cook et al. 2015) and specifically focused on the Mediterranean (Nicault et al. 2008) are also
86 available, the quality of the reconstructions is not spatially homogenous across the studied region,
87 in some case having issues over the IP. At a smaller scale, there are several temperature and
88 precipitation reconstructions in Spain based on TRW (Fernández et al. 1996; Manrique and
89 Fernandez-Cancio 2000; Dorado Liñán et al. 2015; Esper et al. 2015; Tejedor et al. 2015) or tree-
90 ring density chronologies (Buntgen et al. 2008; Dorado Liñán et al. 2012). Some studies used the
91 stable isotopic signatures of IP tree-rings for climate related studies (Andreu Hayles 2007;
92 Andreu et al. 2008; Planells et al. 2009; Andreu-Hayles et al. 2011; Dorado Liñan et al. 2012;
93 Konter et al. 2014; Dorado Liñán et al. 2015).

94 Climate variability in the northwestern IP is associated with the North Atlantic Oscillation (NAO)
95 (Rodó et al. 1997; Rodriguez-Puebla et al. 1998). The NAO, defined by the pressure difference
96 between the Azores High and the Icelandic Low, determines the strength and position of the
97 westerly flow and thus, the main precipitation patterns across Europe, and to a lesser extent in
98 eastern North America, and Africa (Hurrell 1995). It also impacts fish inventories, agriculture,
99 and hydroelectric production through available water resources (Trigo et al. 2004; López-
100 Moreno et al. 2007; Vicente-Serrano and López-Moreno 2008). Although the NAO is considered
101 the dominant mode of interannual variability for European climate, its effect is dominant in
102 winter, as the associated pressure changes during summer are weaker and thus exert less
103 influence on hydroclimate variability (Trigo et al. 2008; Hernández et al. 2015). During summer,
104 storm track activity is reduced and European hydroclimate and in particular heat extremes are
105 often associated with atmospheric blocking situations (Lehmann and Coumou 2015). Links to
106 the Summer North Atlantic Oscillation (SNAO) have been made (Linderholm et al. 2009; Buwen
107 et al. 2013). During a positive SNAO, based on an index of July–August sea level pressure (SLP)
108 variability in the North Atlantic sector, anticyclonic conditions occur over the UK, whereas the
109 Mediterranean area is wet and cloudier (Bladé et al. 2011).

110 Here, we use tree-ring samples from a *Pinus sylvestris* relict forest (García Antón et al. 1997)
111 located at 1600 m.a.s.l in the Cantabrian range near to the village ‘*La Puebla de Lillo*’ (herein
112 Lillo) to infer hydroclimate variability for the last 400 years in northwestern Iberia (Fig. 1).
113 Using three different tree-ring parameters from the same chronology: TRW, carbon ($\delta^{13}\text{C}$) and
114 oxygen ($\delta^{18}\text{O}$) stable isotopes, we applied linear and non-linear methods to determine the
115 climatic signal recorded by these trees. Our findings include significant linkages between distinct

116 tree-ring proxies and regional late spring and summer precipitation associated with specific
117 atmospheric patterns.

118

119 **2 Data and methods**

120 **2.1 The tree-ring chronologies**

121 The TRW, $\delta^{13}\text{C}$ and $\delta^{18}\text{O}$ data presented here have been previously used in studies with
122 different goals (e.g., Treydte et al. 2007; Andreu et al. 2008; Andreu-Hayles et al. 2011;
123 Saurer et al. 2014; Frank et al. 2015). The TRW series were standardised using the residual
124 method with a 250-yr spline (Cook and Kairiukstis 1990) on power transformation (Cook and
125 Peters 1997). Other standardisation, such as the Signal Free method (Melvin and Briffa 2008)
126 or the Friedman super smooth (Friedman 1984), were explored without leading to large
127 differences among the resulting chronologies. In relation to the isotopic analyses, wood from
128 four trees was pooled year by year (Leavitt and Long 1984; Dorado Liñán et al. 2011). The α -
129 cellulose was extracted using sodium hydroxide, sodium chlorite and acetic acid. (Loader et al.
130 1997) and was homogenised using an ultrasonic device (Laumer et al. 2009). Stable isotopes
131 ratios are expressed in the delta (δ) notation in per mil (‰) relative to the standards of the
132 Vienna Pee Dee Belemnite (VPDB) for $\delta^{13}\text{C}$ and the Vienna Standard Mean Ocean Water (V-
133 SMOW) for $\delta^{18}\text{O}$. $\delta^{13}\text{C}$ ratios were measured by combusting the cellulose in an elemental
134 analyser (Fisons NA 1500 NC, Fisons Instruments, Milan, Italy) interfaced with an IRMS
135 (Micromass Optima isotope ratio mass-spectrometer, VG Instruments, Manchester, UK)
136 operating in continuous flow mode. Cellulose from spruce (“Fluka1”, Fluka Chemika, Ord.#
137 22181, Lot. # 380099/1 20200; $\delta^{13}\text{C}_{\text{VPDB}} = -23.03\text{‰}$) and graphite powder (“G5”, 20-40 μm ,
138 purity 99.99%; $\delta^{13}\text{C}_{\text{VPDB}} = -21.16\text{‰}$) were used as laboratory standards for $\delta^{13}\text{C}$ after

139 calibration against IAEA CH-3 (-24.7‰), IAEA-CH7 (-32.15‰) and USGS24 (-16.04‰).
140 The $\delta^{18}\text{O}$ values were measured using high-temperature pyrolysis (1350°C) of cellulose to
141 carbon monoxide in a Thermo Chemical Elemental Analyser (TC/EA) coupled via a ConFlow
142 II open split to the IRMS (Thermo Finnigan Delta Plus XL IRMS). The measurements'
143 reproducibility was better than 0.1‰ and 0.3‰ for $\delta^{13}\text{C}$ and $\delta^{18}\text{O}$ ratios, respectively. The
144 laboratory standards used for $\delta^{18}\text{O}$ were IAEA-C3 cellulose ($32.6 \pm 0.2\text{‰}$), IAEA-CH6 sucrose
145 ($36.4 \pm 0.2\text{‰}$) and Merck cellulose ($28.67 \pm 0.2\text{‰}$) after calibration against V-PDB and
146 converted then to V-SMOW by using $\delta_{\text{VSMOW}} = 1.0415 \delta_{\text{PDB}} + 41.5\text{‰}$ IAEA standards (Borella
147 et al. 1999). In order to remove non-climatic trends from the raw $\delta^{13}\text{C}$ tree-ring data: we
148 applied (1) the atmospheric correction to avoid disturbances due to the Suess effect (increase
149 in ^{13}C -depleted atmospheric CO_2 due to fossil-fuel burning and deforestation since the
150 industrialisation) using the values listed by McCarroll and Loader (2004); (2) the pin
151 correction (McCarroll et al. 2009) to account for the tree ecophysiological response due to
152 higher CO_2 . There are constant fractionation processes affecting the $\delta^{13}\text{C}$ signatures due to
153 CO_2 diffusion through stomata and carboxylation (by Rubisco during photosynthesis), but
154 other fractionations can also occur due to changes in the environmental conditions. These are
155 the signals sought in this paper.

156

157 **2.2 Observational/reanalysis and gridded reconstruction products**

158 A series of monthly global gridded observational and reanalysis products were used to assess
159 regional hydroclimate and the associated large-scale atmospheric conditions that give rise to
160 extremes in the tree-ring proxies. The primary variables that we compare directly with the tree
161 ring proxies are temperature and precipitation at the Lillo study site (box in Fig. 1) that

162 directly affect tree growth and physiological processes. However, an important goal of the
163 paper was to assess the large-scale circulation features that give rise to these two variables
164 representing hydroclimate. It is not implied that trees directly record or are sensitive to SLP
165 anomalies; rather the study aims to advance understanding of tree ring proxy reconstructions
166 by gaining indirect information about large-atmospheric patterns in the past by knowing how
167 the trees respond to hydroclimatic variations.

168 At 2.5° horizontal resolution, these include zonal and meridional winds, and specific humidity
169 from the National Centers for Environmental Prediction (NCEP)/National Center for
170 Atmospheric Research (NCAR) reanalysis (NNR; 1948-present; Kalnay et al. 1996; Kistler et
171 al. 2001) and the 2° horizontal resolution 20th Century reanalysis (20CR; 1871-2011; Compo
172 et al. 2011); precipitation at 0.5° horizontal resolution from the Global Precipitation
173 Climatology Centre (GPCC; version 6; 1901-2010; Schneider et al. 2014) and temperature at
174 0.5° resolution from the Climate Research Unit (CRU TS 2.1; 1901-2002; Mitchell and Jones
175 2005). The common analysis period was taken as 1925-2002 (see section below), though
176 results were repeated for the more recent period post-1957 with improved data coverage.
177 Given the robustness of the results, we only show analyses for the longer period 1925-2002.
178 Prior to the instrumental period, we used two 0.5° resolution gridded products: reconstructions
179 of SLP fields from 1500-1999 (Luterbacher et al. 2002) and the Old World Drought Atlas
180 (OWDA), a set of yearly maps of the reconstructed self-calibrating Palmer Drought Severity
181 Index (scPDSI) for the summer season during the Common Era based on tree rings (Cook et al.
182 2015).

183

184 **2.3 Analysis approach**

185 The calibration period overlapping between the proxies and instrumental data was from 1925 to
186 2002, after excluding the beginning of the 20th century due to continuous extreme low values
187 observed in the TRW chronology. The persistence and magnitude of this disturbance pattern over
188 more than two decade suggest a non-climatic origin. Most of the sampled trees had scars
189 produced by the extraction of torches, an activity that is documented to have occurred in the
190 studied forest from the end of the 19th century to the 1st quarter of the 20th century (Orden
191 Martín 2013). The same analyses performed over the entire possible calibration period (1901-
192 2002) show consistent results with the ones presented here, although some lower climatic
193 sensitivity in some of the proxies was observed (results not shown). The time span used for the
194 pre-instrumental or historical period from 1665 to 1900 was determined by the reliable time-span
195 of the TRW chronology starting in 1663 that was assessed by an Expressed Population Signal
196 statistic higher than 0.85 (Wigley et al. 1984).

197 Time-series of climate data for the Lillo region were created as area-average for the domain
198 delimited by the red box (42.25 to 43.75N; 2.75 to 7.75W) shown in Fig. 1, based on the
199 GPCC precipitation (Schneider et al. 2014) and the CRU temperature (Mitchell and Jones
200 2005) gridded data sets. The initial identification of monthly and seasonal climate signals in
201 the tree-ring data was assessed through correlations (Fig. 2) of the three tree-ring chronologies
202 (Fig. 3) with precipitation, as well as partial correlations with mean temperature data
203 controlling the influence of precipitation using the approach implemented in Seascorr (Meko
204 et al. 2011).

205 An analysis of extremes was used to (1) provide insights on the physiological processes
206 affecting the tree-ring proxies (box plot analyses, Fig. 4); (2) to accommodate non-linear tree-
207 ring responses to variations in hydroclimate with regard to the sign of the anomaly and its

208 seasonality (seasonal cycles; Fig. 5); (3) to understand the seasonal large-scale atmospheric
209 mechanisms associated with these years (composite maps; Fig. 6 and 7). As is customary for
210 non-normally distributed variables, such as precipitation, all values in the three tree-ring proxy
211 time-series were ranked and the lowest/highest decile (i.e. extremes) were selected. This led to
212 a selection of 8 high and 8 low extreme years for the instrumental period 1925-2002 (Table 1)
213 and a total of 23 high and 23 low extreme years for the historical period 1665-1900 (Table 2)
214 comprising 236 years. All extreme years are shown in Fig. 3 (filled circles) and the associated
215 other proxy values for the extreme years are compared using box-and-whisker plots in Fig. 4.
216 We assessed the characteristics of the seasonal cycle of Lillo precipitation and surface air
217 temperature (SAT) during these 8 years with extreme high/low proxy values for the
218 instrumental period, with the coloured lines indicating the mean seasonal cycle for the three
219 parameters (Fig. 5d-i). To determine whether the mean seasonal cycle during these extreme
220 years differs significantly from average years a boot-strapping method (i.e., Monte Carlo test)
221 was employed: for a particular time-series, 8 random years were selected for the period 1925-
222 2002. This was repeated 25,000 times to generate an expected distribution of the seasonal
223 cycle for any given set of 8 years. The grey shading in Fig. 5d-i represents the 90%
224 significance level of this expected distribution for high/low years. Wherever a coloured line
225 lies outside the grey shading, the precipitation or SAT in the extreme years differs
226 significantly from average conditions.

227 Using those same years, composite anomalies (Fig. 6-7) of precipitation, SAT, moisture
228 transport, and SLP were calculated for those months when the seasonal precipitation cycle
229 during extreme years deviates significantly from average rainfall conditions based on all years.
230 A two-tailed *t*-test was used to determine whether composite anomalies of precipitation, SAT,

231 moisture transport, and SLP were significant at the 90% level from the long-term mean based
232 on all years.

233 The years with extreme values in the palaeo proxy time-series (TRW, $\delta^{13}\text{C}$, and $\delta^{18}\text{O}$) for the
234 previous centuries were detected by 2 distinct approaches: (a) decile method: 23 high/low
235 extreme proxy years detected as deciles for the period 1665 to 1900 (Fig. 3, filled circles); (b)
236 threshold method: years with proxy values that exceeded a threshold value determined by the
237 lowest of the uppermost decile and the highest of the lowermost decile of the proxy values in the
238 analysis period 1925-2002 (Table 1; horizontal red/blue line in Fig. 3a-c and Fig. 5a-c; empty
239 circles and crosses in Fig. 3). For those high/low extreme proxy years detected by the threshold
240 method throughout the historical period (1665-1900), composite anomalies were calculated for
241 SLP reconstructed fields over the eastern North Atlantic region and Europe (Luterbacher et al.
242 2002) in Fig. 8 and for PDSI based on the Old World Drought Atlas (OWDA; Cook et al. 2015)
243 in Fig. 9. Composites were also calculated for the 8 high/low extreme years for the instrumental
244 period for validating the method for SLP (Fig. 10) and PDSI (Fig. 11). Fig. 12 shows variations
245 in the number of occurrence of years with extreme events per decade obtained in 20-yr sliding
246 windows for the two isotope proxies. The temporal evolution of extreme events is only shown
247 for the sign, for which strong significant deviations in the seasonal cycle of Lillo precipitation
248 were detected (cf. Fig. 5d-f).

249

250 **3 Distinct climatic signals in the tree ring proxies**

251 The climatic signal recorded by each tree-ring proxy (TRW, $\delta^{13}\text{C}$ and $\delta^{18}\text{O}$) show distinct
252 strength and seasonality (Fig. 2). Tree growth, represented by TRW records, is mildly favoured
253 by wet conditions from April to August (i.e. positive correlation between TRW and

254 precipitation); in contrast the effect of temperature, with the precipitation effect removed, seems
255 to be negligible without a single month with significant correlation. The tree-ring parameter most
256 sensitive to summertime water availability is $\delta^{13}\text{C}$. The $\delta^{13}\text{C}$ records exhibit the highest climate
257 sensitivity with significant negative correlation with June-July precipitation and positive partial
258 correlation with July-August temperatures. The $\delta^{18}\text{O}$ records exhibit weaker correlations, but
259 similar seasonal sensitivity to $\delta^{13}\text{C}$ with negative and positive correlations from May to July
260 precipitation and July to September temperatures, respectively (Fig. 2). Therefore, both stable
261 isotopic ratios ($\delta^{13}\text{C}$ and $\delta^{18}\text{O}$) seem to be mainly modulated by changes in moisture during
262 summer time.

263

264 **4 Physiological processes related to climate variability**

265 The $\delta^{13}\text{C}$ ratios may be lower (ratios depleted in the heavier isotope ^{13}C) during wet summers
266 because more open stomata lead to more CO_2 available in the stomatal chambers. This leads to
267 more discrimination against the heavier isotope, ^{13}C , since the lighter isotope, ^{12}C , is preferred as
268 a substrate for photosynthesis (Farquhar et al. 1982). Dry summers may lead to higher $\delta^{13}\text{C}$
269 values (ratios enriched in ^{13}C) since closer stomata allow less CO_2 availability in the stomatal
270 chambers, and thus discrimination against ^{13}C is lower.

271 An enrichment (depletion) of the $\delta^{13}\text{C}$ isotopic signature due to higher (lower) assimilation rates
272 linked to temperature or light influences on photosynthesis (McCarroll and Pawellek 1998)
273 cannot be initially ruled out. Both physiological processes (i.e. assimilation increase and
274 reduction in stomata conductance) produce the same isotopic signature as a result of
275 reducing/increasing the ^{12}C availability in the stomatal chambers. However, our results show
276 significantly lower and higher $\delta^{13}\text{C}$ ratios during the years with the 8 highest and 8 lowest

277 growth observed (Fig. 4a), respectively. This suggests a stronger regulation by stomatal
278 variations (e.g. close stomata may lead to higher $\delta^{13}\text{C}$ and lower TRW) compared to assimilation
279 (e.g. more photosynthesis may lead to higher $\delta^{13}\text{C}$ and higher TRW).

280 The $\delta^{18}\text{O}$ values are mainly affected by the original values of the $\delta^{18}\text{O}$ of the source water and
281 the fractionation processes at the leaf level through stomatal conductance (Barbour 2007),
282 mechanism explained above for $\delta^{13}\text{C}$. This leads to lower $\delta^{18}\text{O}$ ratios (depleted in heavy isotopes,
283 ^{18}O) during wet summers and to higher $\delta^{18}\text{O}$ ratios (enriched in ^{18}O) during dry summers. During
284 cyclonic wet summers, $\delta^{18}\text{O}$ ratios in cellulose are lower because of low $\delta^{18}\text{O}$ values in rainfall
285 (source water) and a lowered evaporative enrichment process at the leaf level due to lower
286 vapour pressure due to moist air (Young et al. 2015). In contrast during anticyclonic conditions,
287 the opposite fractionation processes occur.

288 Temperatures may also have an independent effect on precipitation supported by the significant
289 partial correlations with both stable isotopic series after removing the influence of precipitation
290 on the tree-ring proxies. Warm and cold summers may enhance the enrichment (high) and
291 depletion (low) of isotopic ratios, respectively, via changes in vapour pressure at leaf level
292 through stomata conductance. In summary, higher $\delta^{13}\text{C}$ and $\delta^{18}\text{O}$ values (~ enriched) document
293 drier and warmer conditions, whereas lower $\delta^{13}\text{C}$ and $\delta^{18}\text{O}$ values (~ depleted) are related to
294 wetter and colder conditions.

295 The years detected by the $\delta^{13}\text{C}$ and $\delta^{18}\text{O}$ extreme values do not always coincide with 6 out of 8
296 and 3 out of 8 matches for wet years and dry years, respectively (Table 1). Despite this, the box
297 plot analyses (Fig. 4) confirm the coherence between both proxies. During the 8 years with the
298 lowest / highest $\delta^{13}\text{C}$ ratios (Fig. 4e), the $\delta^{18}\text{O}$ values were significantly lower and higher,
299 respectively. Likewise during years with the 8 lowest / highest $\delta^{18}\text{O}$ ratios (Fig. 4f), the $\delta^{13}\text{C}$

300 ratios were significantly lower and higher, respectively. A correlation value of 0.58 between the
301 $\delta^{13}\text{C}$ and $\delta^{18}\text{O}$ records supports that summer moisture availability is regulating both isotopes at
302 the leaf level.

303 Nevertheless, other environmental factors are also independently modulating each proxy. The
304 lower climatic sensitivity of $\delta^{18}\text{O}$ compared to $\delta^{13}\text{C}$ records may be partially due to the
305 contribution of the original values of the source water (Saurer et al. 2002) and fractionation
306 processes occurring in this meteoric water until the fixation of the $\delta^{18}\text{O}$ in plant tissue (McCarroll
307 and Loader 2004).

308 **5 Asymmetric moisture signal in high and low extreme proxy years**

309 Figure 5 shows the tree-ring series and seasonal cycle for precipitation and temperature for the
310 study site Lillo (red box in Fig. 1) for the instrumental period 1925-2002. Years recording the
311 highest/lowest 10% of the values in each tree-ring record (i.e. deciles) were selected (blue/red
312 filled circles in Fig. 5 for (a) TRW, (b) $\delta^{13}\text{C}$, and (c) $\delta^{18}\text{O}$), and used to calculate the seasonal
313 cycle in precipitation (d, f) and temperature (g, i). Blue lines illustrate the seasonal cycle for
314 years with high precipitation detected by wide (high) TRW, depleted (low) $\delta^{13}\text{C}$ and depleted
315 (low) $\delta^{18}\text{O}$ values. Red lines show the seasonal cycle for years with low precipitation detected
316 by narrow (low) TRW, enriched (high) $\delta^{13}\text{C}$ and enriched (high) $\delta^{18}\text{O}$. Therefore, significantly
317 wetter conditions than average (blue lines outside the grey band) are detected in June by
318 extreme wide TRW values and in June-July by extreme low $\delta^{13}\text{C}$ and $\delta^{18}\text{O}$ ratios. In contrast,
319 significantly drier conditions (red lines outside the grey band) are detected in June associated
320 with the narrowest TRW and the highest $\delta^{13}\text{C}$, and in May related to extreme high $\delta^{18}\text{O}$ ratios.
321 For the temperature seasonal cycles (g-i), blue lines indicate that these years exhibit low
322 temperatures in July-August detected by depleted (low) $\delta^{13}\text{C}$ and in July by depleted (low)

323 $\delta^{18}\text{O}$. Red lines indicate warm conditions in July and August for years with enriched (high)
324 $\delta^{13}\text{C}$. Extreme wide TRW are significantly related to warm temperatures in April that may
325 favour the onset of the growing season, while narrow TRW seem to be associated, albeit not
326 significantly, with warmer temperatures during June and July.

327 These seasonal cycle analyses indicate that months with significant deviations from average
328 climatic conditions differ between years with extreme high and low proxy values. Thus, timing
329 (years and seasons) of climatic extremes is different for high and low extremes of the same proxy.
330 For instance, in years with extreme high $\delta^{13}\text{C}$ values (Fig. 5b) significantly drier conditions
331 occurred during June (Fig. 5e), but the wetter conditions detected by the low $\delta^{13}\text{C}$ value occurred
332 during July-August (Fig. 5e). Overall, climatic sensitivity is seasonally shifted between proxy
333 high/low values: dry conditions are detected to occur earlier in the year in late spring, while wet
334 conditions are found to occur later more focused on the summer months.

335

336 **6 Atmospheric patterns associated with dry/wet conditions**

337 The months identified by the precipitation seasonal cycle analysis with significant deviations
338 in precipitation from mean conditions are consistent with large-scale atmospheric features
339 described by composite analyses for the same months (Fig. 6-7). Our composite anomaly maps
340 indicate different circulations patterns for high and low extreme years. It should be noted that
341 the composites show anomalies rather than the mean field, so the circulation changes thus
342 relate more to a strengthening or weakening of the westerly onshore moisture transport for
343 example, rather than a complete change in direction and therefore change in source water
344 region.

345

346 **6.1 Wet summer conditions**

347 The seasonal temperature and precipitation cycles in years with extreme low $\delta^{13}\text{C}$ values (Fig. 5b)
348 show significantly colder conditions for July (Fig. 5h) and wetter during June-July (Fig. 5e),
349 respectively. The June-July composites for years with extreme low $\delta^{13}\text{C}$ show significantly
350 wetter and colder conditions for the Cantabrian range, western Iberia and southwestern France
351 (Fig. 6b,e). This is associated with an enhanced onshore moisture transport from the Atlantic
352 Ocean (Fig. 6h) driven by significant positive SLP anomalies at high latitudes and negative
353 anomalies over Europe (Fig. 6k). Similar patterns are found during years with low $\delta^{18}\text{O}$ values
354 (Fig. 5c) with significant anomalies in the precipitation and temperature seasonal cycles detected,
355 corresponding to wetter (Fig. 5f) and colder (Fig. 5i) early summer conditions. Composite
356 anomalies for these years during June-July confirm significantly higher precipitation over the
357 northern IP and southern France (Fig. 6c), enhanced moisture transport from the Atlantic (Fig. 6i)
358 and consistent SLP patterns (Fig. 6l), with significantly colder conditions across the IP (Fig. 6f).
359 The composites corresponding to years with wide TRW values associated with anomalous wet
360 conditions for June in the seasonal cycle (Fig. 5d) show higher precipitation along the northern
361 IP (Fig. 6a), associated with coherent moisture transport (Fig. 6g) and SLP patterns (Fig. 6j), as
362 well as colder temperatures over the IP (Fig. 6d). The moisture transport in years with high TRW
363 values shows more local atmospheric features with moisture coming directly from the west (Fig.
364 6g), resulting in local precipitation events at the study site (Fig. 6a). In contrast, moisture
365 transport patterns associated with the low isotopic values (Fig. 6h, i) exhibit more broad-scale
366 anomalous moisture transport features spanning across western Europe and western North Africa
367 that lead to anomalous precipitation over a larger region of the IP and into southern France (Fig.

368 6b, c). These large-scale patterns detected by extreme isotopic values are associated with
369 anomalous high SLP anomalies over Iceland and low SLP anomalies over Europe.

370

371 **6.2 Dry late spring-early summer conditions**

372 In years with extreme high $\delta^{13}\text{C}$ values (Fig. 5b) significantly drier conditions occurred during
373 June (Fig. 5e) and warmer conditions during July-August (Fig. 5h). In agreement, composite
374 anomaly maps for June for high $\delta^{13}\text{C}$ years indicate significant reductions in precipitation over
375 the northwestern IP (Fig. 7b) and positive temperature anomalies over the IP (Fig. 7e), associated
376 with coherent large-scale atmospheric circulation patterns. Anomalously low SLP over Iceland
377 and Greenland and high SLP anomalies over western and southern Europe (Fig. 7k) result in a
378 reduced moisture transport into the IP (Fig. 7h). In years with extreme high $\delta^{18}\text{O}$ values
379 significantly drier conditions occur in May (Fig. 5f). Accordingly, the associated composite
380 maps for May reveal significant reductions in precipitation over the western IP (Fig. 7c) and
381 positive SAT anomalies across the wider IP and into France (Fig. 7f), associated with coherent
382 large-scale atmospheric circulation patterns. Anomalously low SLP over the North Atlantic and
383 high SLP over Europe (Fig. 7l) result in a reduced moisture transport into the IP (Fig. 7i). While
384 moisture transport composites for high isotopic years (Fig. 7h, i) share again very similar
385 transport patterns, moisture advection detected by low TRW values (Fig. 7g) indicates a
386 particular circulation pattern associated with positive anomalies over Iceland (Fig. 7j), warmer
387 conditions over the central and southern IP (Fig. 7d) and drier conditions over the Pyrenees, but
388 not over Lillo where the trees are located (Fig. 7a).

389

390 **7 Hydroclimate in the pre-instrumental period**

391 Seasonal composites computed for the period 1665 to 1900 using the SLP gridded product
392 (Luterbacher et al. 2002) and the Old World Drought Atlas (Cook et al. 2015) corroborated the
393 detection of wet/dry years in the pre-instrumental period. Table 2 shows the extreme years
394 detected using the two approaches (decile and threshold method). The composite analyses using
395 years from both approaches led to similar results. Thus, herein we just show results derived from
396 the threshold method.

397 The SLP composites computed using years with high TRW (Fig. 8a), low $\delta^{13}\text{C}$ (Fig. 8b) and low
398 $\delta^{18}\text{O}$ (Fig. 8c) represent SLP patterns that are consistent with wet conditions in the IP. In contrast,
399 low TRW (Fig. 8d), high $\delta^{13}\text{C}$ (Fig. 8e) and high $\delta^{18}\text{O}$ (Fig. 8f) show SLP patterns mostly
400 associated with dry conditions over the IP. Overall, pre-instrumental SLP composites (Fig. 8)
401 compare well with SLP instrumental observations (Fig. 7, 8 and 10), mainly showing low and
402 high pressure anomalies over Europe during wet and dry events, respectively. More specifically,
403 the anomalies in the pre-instrumental period resemble the SLP patterns seen during extreme wet
404 summer months well (Fig. 8a-c and 10a-c), while there is less agreement for the dry extremes
405 (Fig. 8d-f and 10d-f). For the latter, the SLP anomalies over central and southern Europe are
406 consistent between the instrumental and pre-instrumental period, while it is the sign and location
407 of maximum SLP anomalies over northern Europe that differ. The OWDA composites (Fig. 8)
408 indicate mainly wet conditions (Fig. 8a-c) for years with high TRW and low isotopic ratios,
409 whereas non-significant or slightly dry conditions occur over the Lillo area (Fig. 8d-f) for years
410 with low TRW and high isotopic ratios. In addition, SLP (1925-1999; Fig. 10) and OWDA
411 (1925-2002; Fig. 11) composites for the instrumental period also show consistent results with the
412 expected dry and wet years depending on low/high extreme values detected in the tree ring
413 proxies. Therefore, these composites corroborate the validity of our approach of using extreme

414 analyses in tree-ring records to explore the occurrence of wet and dry periods prior to the
415 instrumental period.

416 The three tree-ring parameters present distinct sensitivity to summer moisture availability, while
417 high and low extremes exhibit distinct seasonality and an asymmetric moisture signal. Whereas
418 TRW seems to reflect local atmospheric circulation features, stable isotopes share some large-
419 scale atmospheric patterns across the IP and western Europe that are of interest for this study in
420 order to infer changes in water availability over the IP more broadly. Here, we propose a novel
421 non-linear method to explore past hydroclimatic variability based on the analysis of extremes in
422 the isotopic series to detect specific years in the past (Table 2), in which the proxies recorded
423 significant deviations from average hydroclimatic conditions. Thus, the most likely occurrence
424 of years with wet/dry conditions is recorded independently by each tree-ring parameter for the
425 last 400 years, allowing for precise seasonality and attribution to related atmospheric patterns.
426 Specifically, the extreme isotopic values respond to summertime/late spring moisture availability:
427 wet June-July (low $\delta^{13}\text{C}$ and low $\delta^{18}\text{O}$), dry June (high $\delta^{13}\text{C}$) and dry May (high $\delta^{18}\text{O}$). Hence,
428 these isotopic records are used as proxies for informing about northwestern IP hydroclimate
429 variability during late spring/early summer during the period 1665 to 1900 (Fig. 12).

430 A consistent wet period in the second half of the 19th-century is the most prominent feature
431 for the reconstruction of wet summers (Fig. 12a) based on the high occurrence of wet years
432 detected by low values in the isotopic proxies (Table 2). This is reflected in low $\delta^{13}\text{C}$ values
433 for an extended period of time and even more pronounced in low $\delta^{18}\text{O}$ centred around 1850.
434 Undoubtedly, indicators of ‘wetness’ (depleted isotope values), agree on the persistent mid-
435 19th century pluvial. In addition, any ‘dryness’ indicators (enriched isotope values) are absent
436 during that period as shown in the reconstruction of dry late spring-early summer (Fig. 12b).

437 **8 Discussion**

438 The persistent mid-19th century pluvial seen in our reconstruction (Fig. 12) is corroborated by
439 higher than usual precipitation levels reported between 1835 and 1875 in Barcelona (northeast
440 IP) based on a recently published high-quality instrumental record (Prohom et al. 2015), with a
441 6-year record of rainy years (~1840s-1850s), unique in the next 160 years (Rodrigo and
442 Barriendos 2008; Camuffo et al. 2013). Moreover, historical documentation also reported a
443 lack of droughts and more frequent and severe catastrophic floods in the mid-19th century in
444 Iberia (Barriendos and Martin-Vide 1998; Llasat et al. 2005; Barriendos and Rodrigo 2006),
445 ending this period of extreme floods with the 1874 Santa Tecla flash flood in Catalonia with
446 more than 500 deaths (Ruiz-Bellet et al. 2015). This 19th century pluvial period is also
447 confirmed by higher frequency of extreme events, such as strong snowstorms, marine storms,
448 atmospheric convective activity and catastrophic floods, reported without a well-marked
449 seasonality (Barriendos and Martin-Vide 1998). This unusual occurrence of wet years,
450 associated with high atmospheric instability, may result from a prevalent meridional
451 circulation associated with cold air aloft, which – upon contact with warm/humid air masses
452 from the Mediterranean – may trigger torrential rainfall over the IP, especially over the
453 northeastern IP (Barriendos and Martin-Vide 1998). These severe atmospheric events may
454 also be associated with marked negative NAO phases and advection of cooler air aloft,
455 producing strong rainfall events during such a ‘cold phase’ across the entire northern IP, and
456 thus being detectable on both sides: northeastern (i.e. Mediterranean) and northwestern (i.e.
457 Atlantic) IP, where our study site is located.

458 This information based on historic data aligns with the synoptic situation reported in our
459 composite maps from the instrumental and pre-instrumental periods. During the instrumental

460 period, low $\delta^{13}\text{C}$ and $\delta^{18}\text{O}$ years show circulation anomalies that are consistent with this
461 interpretation with anomalous high SLP over Iceland and lower in the mid-latitudes (Fig. 6k,l),
462 leading to anomalous northwesterly moisture transport from the Atlantic onto the IP (Fig. 6h,i).
463 These circulation features are also associated with anomalous cool SAT across the broader IP
464 (Fig. 6e,f). In the pre-instrumental period, the SLP anomaly pattern associated with low $\delta^{18}\text{O}$
465 years during this unusual pluvial period (Fig. 8c) is indicative of the negative NAO conditions
466 suggested above.

467 Nevertheless, not all the atmospheric events occurred synchronically between the Atlantic and
468 the Mediterranean sides of the northern IP. During the late Maunder Minimum (1675-1715)
469 historic data based on Catholic rogation ceremonies from northeastern locations in Catalonia
470 show almost no drought with steady precipitation levels (Barriendos 1997), whereas rogations
471 from locations with a stronger Atlantic influence show drier conditions, such as Toledo and
472 Zamora located in the western IP during spring (Domínguez-Castro et al. 2010) and the Ebro
473 basin (Vicente-Serrano and Cuadrat 2007). This situation may be linked to a prevalent
474 anticyclone associated with cold conditions that may lead to dry weather in the Atlantic region,
475 but to moderate precipitation levels in the Mediterranean side driven by moisture coming from
476 the East. Consistently with the historical findings from the Atlantic side, our late spring-early
477 summer reconstruction (Fig. 12b) indicates higher occurrence of dry years detected by high
478 values in both isotopic records during the late Maunder Minimum.

479 In contrast, other dry periods were co-occurring across the entire northern IP, as for example a
480 drought during 1775-1778, evident in the Ebro basin under a strong Atlantic influence
481 (Vicente-Serrano and Cuadrat 2007). The anomalous climatic conditions extended along the
482 Mediterranean coast and is considered one of the strongest climatic irregularities occurring

483 during the Maldà Oscillation in Catalonia, northeastern IP (Barriendos and Llasat 2003). This
484 period was likely associated with sustained high pressure anomalies over central Europe
485 (Luterbacher et al. 2000), which may have produced a 'blocking' situation preventing the
486 arrival of low pressure systems from the Atlantic Ocean. In our high $\delta^{13}\text{C}$ years indicative of
487 dry June conditions, the SLP anomalies (Fig. 7h, Fig. 8e) show comparable features to such a
488 scenario, which could have led to prolonged droughts in the Western Mediterranean Basin,
489 interspersed with flooding events (Barriendos and Llasat 2003).

490 Overall, our isotopic tree-ring reconstruction shows the most noticeable period with frequent
491 dry summers from 1665 to 1700 considering the total extent spanning until 1900. In agreement,
492 historical data from Toledo Cathedral based on rogations reported the most severe droughts
493 occurring between 1576-1800, whereas almost no droughts were found during the 1800-1900
494 period (Dominguez-Castro et al. 2008). That this period displays a lack of droughts agrees
495 with the 19th century pluvial situation described in Fig. 12a. In addition, years with extreme
496 values in the tree-ring proxies (Table 2) concur with some particular years of extreme droughts
497 described by historical documentation, such as the years 1680 (Domínguez-Castro et al. 2010),
498 1753, 1817 or 1824 (Domínguez-Castro et al. 2012). Finally, the drought period detected by
499 the isotopic tree-ring series during the second half of the 19th century is confirmed by
500 historical proxies showing dry conditions for the Ebro basin during the same period and a
501 strong positive NAO index at the end of the 19th and early 20th century (Vicente-Serrano and
502 Cuadrat 2007) and by instrumental records from Barcelona that show a dry spell from 1878 to
503 1919 (Prohom et al. 2015). From 1880 to 1910 extremely low grain production was reported in
504 Spain that led to strong reductions in food availability during the first years of the 20th century
505 and related impacts as social conflict and migrations (Vicens Vives 1985; Blanco et al. 1986).

506 Although starvation and migration are driven by a myriad of phenomena, including political
507 and social factors, the dry period in the second half of the 19th century may have also played a
508 role in this historically known crisis of subsistence and economic migrations due to hunger,
509 which coincided with the famous Galician, and Asturian migration to South America (Ojeda
510 and San Miguel 1985; Gómez Gómez 1996).

511 To summarise, independent sources (natural and historical) of past climate variability validate
512 our findings that attribute the non-linear moisture signals recorded by extreme tree-ring values
513 to distinct large-scale atmospheric patterns, and they allow for targeted seasonal 400-yr
514 reconstructions of summer hydroclimate for extreme wet and dry conditions independently.

515

516 **9 Conclusions**

517 An almost symmetric seasonal moisture signal was recorded during years with highest/lowest
518 $\delta^{13}\text{C}$ values, with precipitation anomalies being significant for similar months (Fig. 5e). This
519 explains the robust and strong linear relationship between $\delta^{13}\text{C}$ and precipitation seen in
520 correlations (Fig. 2). An opposite behaviour may render the weaker precipitation signal held by
521 the other tree-ring parameters. TRW and $\delta^{18}\text{O}$ series show a much more marked seasonal
522 asymmetry in their moisture signal. These analyses of extremes revealed that high/low proxy
523 values do not necessarily correspond to mirror images in the atmospheric anomaly patterns,
524 suggesting different drivers and seasonality associated with asymmetric moisture signatures in
525 the proxies, and thus hampering the strength of their climate signal when linear approaches are
526 used (Fig. 2).

527 Severe flooding and droughts are likely to become more frequent with an intensifying water
528 cycle in a warmer world (Wentz et al. 2007; Trenberth 2011; Hartmann et al. 2013). For

529 sustainable water resources management, information about past hydroclimatic changes are
530 needed. Our approach determining the frequency of extreme climatic conditions in the past is a
531 step forward towards a more realistic range of past climate variability considering that the
532 standard methodology based on linear regressions are biased towards the mean climate and often
533 underestimate extremes (McCarroll et al. 2015). Extreme analyses point to a better mechanistic
534 understanding of links between tree-ring proxies and large-scale atmospheric dynamics and can
535 improve climate reconstructions based on proxies with asymmetric and non-stationary signals.
536 Since this information is not available with a traditional linear approach, non-linear methods in
537 palaeoclimate research are useful to overcome the complexity of reconstructing atmospheric
538 features. The distinct seasonal signal in stable isotopes and ring-width supports multi-parameter
539 approaches for advances in the field.

540

541 **Acknowledgements**

542 We thank Oriol Bosch and Octavi Planells for their participation in sampling and laboratory
543 work. Use of the following data sets is gratefully acknowledged: Global Precipitation
544 Climatology Center data by the German Weather Service (DWD) accessed through
545 <http://gpcc.dwd.de>; TS by the Climate Research Unit at the University of East Anglia; NNR
546 data provided by NOAA/OAR/ESRL PSD, Boulder, Colorado, USA, through their website
547 <http://www.cdc.noaa.gov>; and the 20CR Project supported by the U.S. DOE, Office of Science
548 Innovative and Novel Computational Impact on Theory and Experiment program, and Office
549 of Biological and Environmental Research, and by the NOAA Climate Program Office. This
550 research was partially supported by the EU project ISONET (Contract EV K2-2001-00237)
551 and the EU FP6 project Millennium (GOCE 017008). L.A.H. was supported by the *Marie*

552 *Curie International Outgoing Fellowship PIOF-GA-2009-253277* grant within the FP7-
553 PEOPLE-2009-IOF program. CCU was supported by the the *Penzance* and *John P. Chase*
554 *Memorial Endowed Funds* and the *Investment in Science Fund* at WHOI.

555

556 **REFERENCES**

- 557 Andreu Hayles L (2007) Climate and atmospheric CO₂ effects on Iberian pine forests assessed
558 by tree-ring chronologies and their potential for climatic reconstructions. University of
559 Barcelona
- 560 Andreu L, Planells O, Gutiérrez E, Helle G, Schleser GH (2008) Climatic significance of tree-
561 ring width and $\delta^{13}\text{C}$ in a Spanish pine forest network *Tellus Series B-Chemical and*
562 *Physical Meteorology* 60:771-781
- 563 Andreu-Hayles L, Planells O, Gutiérrez E, Muntan E, Helle G, Anchukaitis KJ, Schleser GH
564 (2011) Long tree-ring chronologies reveal 20th century increases in water-use efficiency
565 but no enhancement of tree growth at five Iberian pine forests *Global Change Biology*
566 17:2095-2112 doi:10.1111/j.1365-2486.2010.02373.x
- 567 Barbour MM (2007) Stable oxygen isotope composition of plant tissue: a review *Functional*
568 *Plant Biology* 34:83-94 doi:<http://dx.doi.org/10.1071/FP06228>
- 569 Barriendos M (1997) Climatic variations in the Iberian Peninsula during the late Maunder
570 Minimum (AD 1675-1715): an analysis of data from rogation ceremonies *The Holocene*
571 7:105-111 doi:10.1177/095968369700700110
- 572 Barriendos M, Llasat MC (2003) The Case of the 'Maldá' Anomaly in the Western
573 Mediterranean Basin (AD 1760–1800): An Example of a Strong Climatic Variability
574 *Climatic Change* 61:191-216 doi:10.1023/a:1026327613698
- 575 Barriendos M, Martin-Vide J (1998) Secular Climatic Oscillations as Indicated by Catastrophic
576 Floods in the Spanish Mediterranean Coastal Area (14th–19th Centuries) *Climatic*
577 *Change* 38:473-491 doi:10.1023/a:1005343828552

578 Barriendos M, Rodrigo FS (2006) Study of historical flood events on Spanish rivers using
579 documentary data *Hydrological Sciences Journal* 51:765-783 doi:10.1623/hysj.51.5.765

580 Bladé I, Liebmann B, Fortuny D, Oldenborgh GJ (2011) Observed and simulated impacts of the
581 summer NAO in Europe: implications for projected drying in the Mediterranean region
582 *Climate Dynamics* 39:709-727 doi:10.1007/s00382-011-1195-x

583 Blanco A et al. (1986) *Historia de España*, . Historia 16, ISBN 84-85229-81-9 edn., Madrid

584 Borella S, Leuenberger M, Saurer M (1999) Analysis of delta O-18 in tree rings: Wood-cellulose
585 comparison and method dependent sensitivity *Journal of Geophysical Research-*
586 *Atmospheres* 104:19267-19273

587 Buntgen U, Frank D, Grudd H, Esper J (2008) Long-term summer temperature variations in the
588 Pyrenees *Climate Dynamics* 31:615-631 doi:10.1007/s00382-008-0390-x

589 Buwen D, Rowan TS, Tim W, Kevin H (2013) Variability of the North Atlantic summer storm
590 track: mechanisms and impacts on European climate *Environmental Research Letters*
591 8:034037

592 Cai W, Cowan T, Thatcher M (2012) Rainfall reductions over Southern Hemisphere semi-arid
593 regions: the role of subtropical dry zone expansion *Scientific Reports* 2
594 doi:10.1038/srep00702

595 Camuffo D et al. (2013) Western Mediterranean precipitation over the last 300 years from
596 instrumental observations *Climatic Change* 117:85-101 doi:10.1007/s10584-012-0539-9

597 Compo GP et al. (2011) The Twentieth Century Reanalysis Project *Quarterly Journal of the*
598 *Royal Meteorological Society* 137:1-28 doi:10.1002/qj.776

599 Cook ER, D'Arrigo RD, Mann ME (2002) A Well-Verified, Multiproxy Reconstruction of the
600 Winter North Atlantic Oscillation Index since a.d. 1400* *Journal of Climate* 15:1754-
601 1764 doi:10.1175/1520-0442(2002)015<1754:awvmro>2.0.co;2

602 Cook ER, Kairiukstis L (1990) *Methods of Dendrochronology in Applications in the*
603 *Environmental Sciences* Kluwer, Dordrecht, 394 pp.,

604 Cook ER, Peters K (1997) Calculating unbiased tree-ring indices for the study of climatic and
605 environmental change *Holocene* 7:359–368

606 Cook ER et al. (2015) Old World megadroughts and pluvials during the Common Era *Science*
607 *Advances* 1 doi:10.1126/sciadv.1500561

608 De Luis M, Carlos Gonzalez-Hidalgo J, Longares LA, Stepanek P (2009) Seasonal precipitation
609 trends in the Mediterranean Iberian Peninsula in second half of 20th century *Int J*
610 *Climatol* 29:1312-1323 doi:10.1002/joc.1778

611 Domínguez-Castro F, García-Herrera R, Ribera P, Barriendos M (2010) A shift in the spatial
612 pattern of Iberian droughts during the 17th century *Clim Past* 6:553-563 doi:10.5194/cp-
613 6-553-2010

614 Domínguez-Castro F, Ribera P, García-Herrera R, Vaquero JM, Barriendos M, Cuadrat JM,
615 Moreno JM (2012) Assessing extreme droughts in Spain during 1750–1850 from
616 rogation ceremonies *Clim Past* 8:705-722 doi:10.5194/cp-8-705-2012

617 Dominguez-Castro F, Santisteban JI, Barriendos M, Mediavilla R (2008) Reconstruction of
618 drought episodes for central Spain from rogation ceremonies recorded at the Toledo
619 Cathedral from 1506 to 1900: A methodological approach *Global and Planetary Change*
620 63:230-242 doi:10.1016/j.gloplacha.2008.06.002

621 Dorado Liñán I et al. (2012) Estimating 750 years of temperature variations and uncertainties in
622 the Pyrenees by tree-ring reconstructions and climate simulations *Clim Past* 8:919-933
623 doi:10.5194/cp-8-919-2012

624 Dorado Liñán I, Gutiérrez E, Andreu-Hayles L, Heinrich I, Helle G (2012) Potential to explain
625 climate from tree rings in the south of the Iberian Peninsula *Climate Research* 55:121-
626 136 doi:10.3354/cr01126

627 Dorado Liñán I et al. (2011) Pooled versus separate measurements of tree-ring stable isotopes
628 *Science of The Total Environment* 409:2244-2251

629 Dorado Liñán I et al. (2015) Eight-hundred years of summer temperature variations in the
630 southeast of the Iberian Peninsula reconstructed from tree rings *Climate Dynamics* 44:75-
631 93 doi:10.1007/s00382-014-2348-5

632 Esper J et al. (2015) Atlantic and Mediterranean synoptic drivers of central Spanish juniper
633 growth *Theoretical and Applied Climatology* 121:571-579 doi:10.1007/s00704-014-
634 1254-4

635 Farquhar GD, O’Leary MH, Berry JA (1982) On the Relationship between Carbon Isotope
636 Discrimination and the Intercellular Carbon Dioxide Concentration in Leaves *Australian*
637 *Journal of Plant Physiology* 9:121-137

638 Fernández A, Génova M, Creus J, Gutiérrez E (1996) Dendroclimatological investigations
639 covering the last 300 years in Central Spain. . In: *Tree Rings, Environment and Humanity*
640 (eds. Dean JS, Meko DM, Swetman TW), pp. 181-190 *RADIOCARBON*. 889 pp.

641 Frank DC et al. (2015) Water-use efficiency and transpiration across European forests during the
642 Anthropocene *Nature Clim Change* 5:579-583 doi:10.1038/nclimate2614

643 <http://www.nature.com/nclimate/journal/v5/n6/abs/nclimate2614.html> -

644 [supplementary-information](#)

645 Friedman JH (1984) A variable span scatterplot smoother. Laboratory for Computational
646 Statistics. Stanford University Technical Report No. 5.

647 Fritts H (1976) Tree rings and climate. Academic Press, New York , 433 pp.,

648 Gagen M, McCarroll D, Jalkanen R, Loader NJ, Robertson I, Young GHF (2012) A rapid
649 method for the production of robust millennial length stable isotope tree ring series for
650 climate reconstruction Global and Planetary Change 82–83:96-103
651 doi:<http://dx.doi.org/10.1016/j.gloplacha.2011.11.006>

652 García Antón M, Franco Múgica F, Maldonado J, Morla Juaristi C, Sainz Ollero H (1997) New
653 data concerning the evolution of the vegetation in Lillo pinewood (Leon, Spain) J
654 Biogeogr 24:929-934 doi:10.1046/j.1365-2699.1997.00181.x

655 Giorgi F (2006) Climate change hot-spots Geophys Res Lett 33

656 Giorgi F, Lionello P (2008) Climate change projections for the Mediterranean region Global and
657 Planetary Change 63:90-104

658 Gómez Gómez P (1996) De Asturias a América, Cuba (1850-1930): la comunidad asturiana de
659 Cuba. . Ed. Pedro Gómez Gómez, Oviedo

660 Hartmann DL et al. (2013) Observations: Atmosphere and Surface. In: Stocker TF, D. Qin, G.-K.
661 Plattner, M. Tignor, S.K. Allen, J. Boschung, A. Nauels, Y. Xia, V. Bex and P.M.
662 Midgley (eds.) (ed) Climate Change 2013: The Physical Science Basis. Contribution of
663 Working Group I to the Fifth Assessment Report of the Intergovernmental Panel on
664 Climate Change Cambridge University Press, Cambridge, United Kingdom and New
665 York, NY, USA.,

666 Hernández A et al. (2015) Sensitivity of two Iberian lakes to North Atlantic atmospheric
667 circulation modes *Climate Dynamics* 45:3403-3417 doi:10.1007/s00382-015-2547-8

668 Hoerling M et al. (2012) Anatomy of an Extreme Event *Journal of Climate* 26:2811-2832
669 doi:10.1175/jcli-d-12-00270.1

670 Hurrell JW (1995) Decadal Trends in the North Atlantic Oscillation: Regional Temperatures and
671 Precipitation *Science* 269:676-679

672 Kalnay E et al. (1996) The NCEP/NCAR 40-Year Reanalysis Project *Bulletin of the American*
673 *Meteorological Society* 77:437-471 doi:10.1175/1520-
674 0477(1996)077<0437:tnyrp>2.0.co;2

675 Karauskas KB, Ummenhofer CC (2014) On the dynamics of the Hadley circulation and
676 subtropical drying *Climate Dynamics* 42:2259-2269 doi:10.1007/s00382-014-2129-1

677 Kistler R et al. (2001) The NCEP–NCAR 50–Year Reanalysis: Monthly Means CD–ROM and
678 Documentation *Bulletin of the American Meteorological Society* 82:247-267
679 doi:10.1175/1520-0477(2001)082<0247:tnnyrm>2.3.co;2

680 Konter O, Holzkämper S, Helle G, Büntgen U, Saurer M, Esper J (2014) Climate sensitivity and
681 parameter coherency in annually resolved $\delta^{13}\text{C}$ and $\delta^{18}\text{O}$ from *Pinus uncinata* tree-ring
682 data in the Spanish Pyrenees *Chemical Geology* 377:12-19
683 doi:<http://dx.doi.org/10.1016/j.chemgeo.2014.03.021>

684 Labuhn I et al. (2014) Tree age, site and climate controls on tree ring cellulose $\delta^{18}\text{O}$: A case
685 study on oak trees from south-western France *Dendrochronologia* 32:78-89
686 doi:<http://dx.doi.org/10.1016/j.dendro.2013.11.001>

687 Lau WKM, Kim KM (2015) Robust Hadley Circulation changes and increasing global dryness
688 due to CO₂ warming from CMIP5 model projections *Proceedings of the National*

689 Academy of Sciences of the United States of America 112:3630-3635
690 doi:10.1073/pnas.1418682112

691 Laumer W, Andreu L, Helle G, Schleser GH, Wieloch T, Wissel H (2009) A novel approach for
692 the homogenization of cellulose to use micro-amounts for stable isotope analyses Rapid
693 Communications in Mass Spectrometry 23:1934-1940

694 Leavitt SW, Long A (1984) Sampling strategy for stable carbon isotope analyses of tree rings in
695 pine Nature 311:145-147

696 Lehmann J, Coumou D (2015) The influence of mid-latitude storm tracks on hot, cold, dry and
697 wet extremes Scientific Reports 5:17491 doi:10.1038/srep17491
698 <http://www.nature.com/articles/srep17491-supplementary-information>

699 Linderholm HW, Folland CK, Walther A (2009) A multicentury perspective on the summer
700 North Atlantic Oscillation (SNAO) and drought in the eastern Atlantic Region Journal of
701 Quaternary Science 24:415-425 doi:10.1002/jqs.1261

702 Llamas MR (2003) Lessons learnt from the impact of the neglected role of groundwater in
703 Spain's water policy. Water Resources Perspectives: Evaluation, Management, and
704 Policy, A. S. Sharhan and W. W. Wood, Eds., Elsevier Science, Amsterdam, 63–81.

705 Llasat M-C, Barriendos M, Barrera A, Rigo T (2005) Floods in Catalonia (NE Spain) since the
706 14th century. Climatological and meteorological aspects from historical documentary
707 sources and old instrumental records Journal of Hydrology 313:32-47
708 doi:<http://dx.doi.org/10.1016/j.jhydrol.2005.02.004>

709 Loader NJ, Robertson I, Barker AC, Switsur VR, Waterhouse JS (1997) An improved technique
710 for the batch processing of small wholewood samples to α -cellulose Chemical Geology
711 136:313-317

712 Loader NJ, Young GHF, Grudd H, McCarroll D (2013) Stable carbon isotopes from Torneträsk,
713 northern Sweden provide a millennial length reconstruction of summer sunshine and its
714 relationship to Arctic circulation *Quaternary Science Reviews* 62:97-113
715 doi:<http://dx.doi.org/10.1016/j.quascirev.2012.11.014>

716 López-Moreno JI, Beguería S, Vicente-Serrano SM, García-Ruiz JM (2007) Influence of the
717 North Atlantic Oscillation on water resources in central Iberia: Precipitation, streamflow
718 anomalies, and reservoir management strategies *Water Resources Research* 43:W09411
719 doi:10.1029/2007wr005864

720 Lu J, Deser C, Reichler T (2009) Cause of the widening of the tropical belt since 1958
721 *Geophysical Research Letters* 36 doi:10.1029/2008gl036076

722 Lu J, Vecchi GA, Reichler T (2007) Expansion of the Hadley cell under global warming
723 *Geophysical Research Letters* 34:L06805 doi:10.1029/2006gl028443

724 Luterbacher J et al. (2000) Monthly mean pressure reconstruction for the Late Maunder
725 Minimum Period (AD 1675–1715) *Int J Climatol* 20:1049-1066 doi:10.1002/1097-
726 0088(200008)20:10<1049::aid-joc521>3.0.co;2-6

727 Luterbacher J et al. (2002) Reconstruction of sea level pressure fields over the Eastern North
728 Atlantic and Europe back to 1500 *Climate Dynamics* 18:545-561 doi:10.1007/s00382-
729 001-0196-6

730 Manrique E, Fernandez-Cancio A (2000) Extreme climatic events in dendroclimatic
731 reconstructions from Spain *Climatic Change* 44:123-138

732 McCarroll D et al. (2009) Correction of tree ring stable carbon isotope chronologies for changes
733 in the carbon dioxide content of the atmosphere *Geochimica Et Cosmochimica Acta*
734 73:1539-1547 doi:10.1016/j.gca.2008.11.041

735 McCarroll D, Loader NJ (2004) Stable isotopes in tree rings *Quaternary Research Reviews*
736 23:771-801

737 McCarroll D, Pawellek F (1998) Stable carbon isotope ratios of latewood cellulose in *Pinus*
738 *sylvestris* from northern Finland: variability and signal-strength *Holocene* 8:675-684
739 doi:10.1191/095968398675987498

740 McCarroll D, Young GH, Loader NJ (2015) Measuring the skill of variance-scaled climate
741 reconstructions and a test for the capture of extremes *The Holocene* 25:618-626
742 doi:10.1177/0959683614565956

743 Meko DM, Touchan R, Anchukaitis KJ (2011) Seascorr: A MATLAB program for identifying
744 the seasonal climate signal in an annual tree-ring time series *Computers & Geosciences*
745 37:1234-1241 doi:<http://dx.doi.org/10.1016/j.cageo.2011.01.013>

746 Melvin TM, Briffa KR (2008) A "signal-free" approach to dendroclimatic standardisation
747 *Dendrochronologia* 26:71-86

748 Mitchell TD, Jones PD (2005) An improved method of constructing a database of monthly
749 climate observations and associated high-resolution grids *Int J Climatol* 25:693-712

750 Naulier M et al. (2015) A millennial summer temperature reconstruction for northeastern Canada
751 using oxygen isotopes in subfossil trees *Clim Past* 11:1153-1164 doi:10.5194/cp-11-
752 1153-2015

753 Nicault A, Alleaume S, Brewer S, Carrer M, Nola P, Guiot J (2008) Mediterranean drought
754 fluctuation during the last 500 years based on tree-ring data *Climate Dynamics* 31:227-
755 245 doi:10.1007/s00382-007-0349-3

756 Ojeda G, San Miguel JL (1985) *Campesinos, emigrantes, indianos Emigración y economía en*
757 *Asturias, 1830-1930. . Salinas, Ed. Ayalga. ISBN 84-7411-132-3.,*

- 758 Orden Martín R (2013) El pinar de Lillo. Bedia Artes Gráficas, S. C. Santander (Cantabria,
759 Spain), 90 pp. ISBN: 978-84-695-6855-2.
- 760 Pauling A, Luterbacher J, Casty C, Wanner H (2006) Five hundred years of gridded high-
761 resolution precipitation reconstructions over Europe and the connection to large-scale
762 circulation *Climate Dynamics* 26:387-405
- 763 Planells O, Gutiérrez E, Helle G, Schleser G (2009) A forced response to twentieth century
764 climate conditions of two Spanish forests inferred from widths and stable isotopes of tree
765 rings *Climatic Change* 97:229-252 doi:10.1007/s10584-009-9602-6
- 766 Previdi M, Liepert BG (2007) Annular modes and Hadley cell expansion under global warming
767 *Geophysical Research Letters* 34:L22701 doi:10.1029/2007gl031243
- 768 Prohom M, Barriendos M, Sanchez-Lorenzo A (2015) Reconstruction and homogenization of the
769 longest instrumental precipitation series in the Iberian Peninsula (Barcelona, 1786–2014)
770 *Int J Climatol*:n/a-n/a doi:10.1002/joc.4537
- 771 Rodó X, Baert E, Comin FA (1997) Variations in seasonal rainfall in Southern Europe during the
772 present century: relationship with the North Atlantic Oscillation and the El Niño-
773 Southern Oscillation *Climate Dynamics* 13:275-284
- 774 Rodrigo FS, Barriendos M (2008) Reconstruction of seasonal and annual rainfall variability in
775 the Iberian peninsula (16th–20th centuries) from documentary data *Global and Planetary*
776 *Change* 63:243-257 doi:<http://dx.doi.org/10.1016/j.gloplacha.2007.09.004>
- 777 Rodriguez-Puebla C, Encinas AH, Nieto S, Garmendia J (1998) Spatial and temporal patterns of
778 annual precipitation variability over the Iberian Peninsula *Int J Climatol* 18:299-316
779 doi:10.1002/(sici)1097-0088(19980315)18:3<299::aid-joc247>3.0.co;2-l

780 Ruiz-Bellet JL, Balasch JC, Tuset J, Barriendos M, Mazon J, Pino D (2015) Historical,
781 hydraulic, hydrological and meteorological reconstruction of 1874 Santa Tecla flash
782 floods in Catalonia (NE Iberian Peninsula) *Journal of Hydrology* 524:279-295
783 doi:<http://dx.doi.org/10.1016/j.jhydrol.2015.02.023>

784 Saurer M, Schweingruber F, Vaganov EA, Shiyatov SG, Siegwolf R (2002) Spatial and temporal
785 oxygen isotope trends at the northern tree-line in Eurasia *Geophysical Research Letters*
786 29:7-1-7-4 doi:10.1029/2001GL013739

787 Saurer M et al. (2014) Spatial variability and temporal trends in water-use efficiency of
788 European forests *Global Change Biology* 20:3700-3712 doi:10.1111/gcb.12717

789 Schneider U, Becker A, Finger P, Meyer-Christoffer A, Ziese M, Rudolf B (2014) GPCC's new
790 land surface precipitation climatology based on quality-controlled in situ data and its role
791 in quantifying the global water cycle *Theoretical and Applied Climatology* 115:15-40
792 doi:10.1007/s00704-013-0860-x

793 Seftigen K, Linderholm HW, Loader NJ, Liu Y, Young GHF (2011) The influence of climate on
794 $^{13}\text{C}/^{12}\text{C}$ and $^{18}\text{O}/^{16}\text{O}$ ratios in tree ring cellulose of *Pinus sylvestris* L. growing in the
795 central Scandinavian Mountains *Chemical Geology* 286:84-93
796 doi:<http://dx.doi.org/10.1016/j.chemgeo.2011.04.006>

797 Tejedor E, de Luis M, Cuadrat J, Esper J, Saz M (2015) Tree-ring-based drought reconstruction
798 in the Iberian Range (east of Spain) since 1694 *International Journal of*
799 *Biometeorology*:1-12 doi:10.1007/s00484-015-1033-7

800 Trenberth K (2011) Changes in precipitation with climate change *Climate Research* 47:123-138
801 doi:10.3354/cr00953

802 Treydte K et al. (2007) Signal strength and climate calibration of a European tree-ring isotope
803 network Geophysical Research Letters 34:L24302 doi:10.1029/2007gl031106

804 Trigo RM, Pozo-Vázquez D, Osborn TJ, Castro-Díez Y, Gámiz-Fortis S, Esteban-Parra MJ
805 (2004) North Atlantic oscillation influence on precipitation, river flow and water
806 resources in the Iberian Peninsula Int J Climatol 24:925-944 doi:10.1002/joc.1048

807 Trigo RM, Valente MA, Trigo IF, Miranda PMA, Ramos AM, Paredes D, García-Herrera R
808 (2008) The Impact of North Atlantic Wind and Cyclone Trends on European
809 Precipitation and Significant Wave Height in the Atlantic Annals of the New York
810 Academy of Sciences 1146:212-234 doi:10.1196/annals.1446.014

811 Vicens Vives J (1985) Historia económica de España. In., ISBN 84-316-1106-5. edn. Vicens
812 Vives Ed. , Barcelona, 8th edition, p 782

813 Vicente-Serrano SM (2006) Spatial and temporal analysis of droughts in the Iberian Peninsula
814 (1910–2000) Hydrological Sciences Journal 51:83-97 doi:10.1623/hysj.51.1.83

815 Vicente-Serrano SM, Cuadrat JM (2007) North Atlantic oscillation control of droughts in north-
816 east Spain: evaluation since 1600 A. D Climatic Change 85:357-379 doi:10.1007/s10584-
817 007-9285-9

818 Vicente-Serrano SM, López-Moreno JI (2008) Nonstationary influence of the North Atlantic
819 Oscillation on European precipitation Journal of Geophysical Research: Atmospheres
820 113:D20120 doi:10.1029/2008jd010382

821 Wentz FJ, Ricciardulli L, Hilburn K, Mears C (2007) How much more rain will global warming
822 bring? Science 317:233-235 doi:10.1126/science.1140746

823 Wigley TML, Briffa KR, Jones PD (1984) On the Average Value of Correlated Time Series,
824 with Applications in Dendroclimatology and Hydrometeorology *Journal of Climate and*
825 *Applied Meteorology* 23:201-213

826 Young GHF et al. (2015) Oxygen stable isotope ratios from British oak tree-rings provide a
827 strong and consistent record of past changes in summer rainfall *Climate Dynamics*
828 45:3609-3622 doi:10.1007/s00382-015-2559-4

829

830

831

832 **TABLES**

833 **Table 1** Years with extreme values in the top and bottom deciles (10%): the ranked 8 highest
 834 and 8 lowest values for the time-series of the Lillo tree-ring chronologies for the period 1925–
 835 2002 for (left) TRW, (middle) $\delta^{13}\text{C}$, and (right) $\delta^{18}\text{O}$. The lowest of the uppermost decile and
 836 the highest of the lowermost decile of the proxy values are highlighted in grey and were used
 837 as thresholds for analyses in the pre-instrumental period.

Wet years					
Year	High TRW	Year	Low d13C	Year	Low d18O
1959	1.30	1958	-22.62	1930	29.60
1955	1.29	1930	-22.63	1953	29.53
1973	1.27	1977	-22.65	1957	29.38
1956	1.24	1966	-22.66	1931	29.26
1971	1.24	1932	-22.69	1925	29.22
1958	1.21	1925	-22.70	1932	29.16
1953	1.21	1952	-22.71	1952	28.97
1936	1.21	1931	-22.86	1977	28.46

Dry years					
Year	Low TRW	Year	High d13C	Year	High d18O
1948	0.87	1991	-20.67	2001	32.71
1982	0.86	1994	-20.91	2002	32.18
2001	0.84	1999	-20.95	1986	32.12
1986	0.83	1989	-20.97	1958	32.08
1983	0.83	2001	-20.99	1963	32.08
1925	0.80	1986	-21.04	1990	32.06
1991	0.80	1990	-21.04	1995	32.00
1984	0.79	1979	-21.11	1965	31.95

838

839

840 **Table 2** Years with extreme values in the top and bottom deciles (10%): the 23 highest and 23
841 lowest values for the time-series of the Lillo tree-ring chronologies for the period 1665–1900
842 for (left) TRW, (middle) $\delta^{13}\text{C}$, and (right) $\delta^{18}\text{O}$. Years with proxy values above or below the
843 thresholds (horizontal lines in Fig. 3) established in the instrumental period (1925-2002) by the
844 lowest of the uppermost decile and the highest of the lowermost decile of the proxy values
845 (Table 1) are indicated: (a) grey boxes: when those years overlapped with the 23 years within
846 the deciles; (b) listed at the end just for TRW: when those years are different from the 23 years
847 within the deciles.

848

Wet years			Dry years		
High TRW	Low d13C	Low d18O	Low TRW	High d13C	High d18O
(a) Years with extreme values in the top/bottom decils (10%) from 1665 to 1900					
1672	1708	1684	1705	1669	1670
1673	1721	1714	1706	1674	1686
1680	1747	1745	1707	1678	1696
1682	1749	1747	1709	1680	1699
1690	1756	1749	1741	1681	1700
1691	1758	1755	1756	1682	1702
1692	1801	1768	1767	1683	1705
1693	1808	1788	1768	1688	1730
1694	1809	1799	1769	1694	1738
1715	1825	1800	1770	1696	1741
1718	1826	1806	1771	1703	1748
1734	1836	1823	1800	1712	1753
1737	1841	1843	1803	1716	1784
1866	1843	1845	1804	1726	1785
1867	1845	1849	1806	1729	1824
1868	1849	1853	1824	1731	1828
1869	1850	1854	1826	1738	1868
1870	1852	1855	1841	1771	1870
1871	1858	1878	1844	1776	1873
1878	1877	1880	1845	1778	1874
1881	1885	1883	1849	1817	1881
1892	1887	1885	1855	1832	1898
1893	1888	1889	1856	1898	1899

(b) Years with extreme values outside the decile range (10%) from 1665 to 1900

1670, 1681	1705, 1706
1684, 1695	1707, 1708
1696, 1727	1723, 1724
1730, 1762	1755, 1757
1882	1801, 1817
	1823, 1827
	1836, 1840
	1842

849

1 **400 years of summer hydroclimate from**
2 **stable isotopes in Iberian trees**

3 LAIA ANDREU-HAYLES *

4 CAROLINE C. UMMENHOFER, MARIANO BARRIENDOS

GERD HELLE, GERHARD H. SCHLESER, MARKUS LEUENBERGER, EMILIA GUTIÉRREZ

AND EDWARD R. COOK

5 **FIGURES**

under revision in Climate Dynamics

* *Corresponding author address:* Laia Andreu-Hayles, Tree-Ring Laboratory, Lamont-Doherty Earth Observatory, Columbia University, Palisades, NY, USA; lah@ldeo.columbia.edu

6 List of Figures

- 7 1 Mean observed annual precipitation (mm) in the Iberian Peninsula for the
8 period 1901–2002: The Lillo study site (star) and other key locations are
9 indicated. Red dashed box delimits the target region used to create the Lillo
10 precipitation and temperature time series used in this study. 4
- 11 2 Correlations for monthly precipitation and partial correlations for tempera-
12 ture, both from October in the previous year to September of the current year
13 for the period 1925–2002 with tree-ring parameters for (left) TRW, (middle)
14 $\delta^{13}\text{C}$, and (right) $\delta^{18}\text{O}$. Note that coloured bars indicate significant correla-
15 tion coefficients at the 95% confidence level. 5
- 16 3 Time-series of the Lillo tree-ring chronologies for the period 1600–2002 for
17 (a) TRW, (b) $\delta^{13}\text{C}$, and (c) $\delta^{18}\text{O}$. The circles in the period from 1665 to
18 1900 show the years with extreme values in the top and bottom deciles of
19 the proxy times-series: the 23 highest and 23 lowest values (Table 2). Filled
20 circles indicate that the values are above or below the thresholds (horizontal
21 lines) established in the instrumental period by the lowest of the uppermost
22 decile and the highest of the lowermost decile of the proxy values in the
23 analysis period 1925–2002 (Table 1). Dashed lines delineate the studied pre-
24 instrumental period from 1665 to 1900 and the instrumental period from 1925
25 to 2002 used for the analyses shown in Figs. 5-7 7
- 26 4 Box-and-whisker plots for the values of the tree-ring records during the 8 years
27 of extreme high/low values for each tree-ring records: (left) TRW, (middle)
28 $\delta^{13}\text{C}$ and (right) $\delta^{18}\text{O}$. The red line represents the median, the blue boxes
29 delimit the 25th and 75th percentile (i.e. interquartile range) and whiskers
30 the minimum and maximum values. 8

- 31 5 Lillo tree-ring series and seasonal cycles for precipitation and temperature:
32 (a-c) Time-series of the Lillo tree-ring chronologies for the period 1925–2002
33 for (left) TRW, (middle) $\delta^{13}\text{C}$, and (right) $\delta^{18}\text{O}$. Annual values are shown in
34 black, 5-year moving average in green, and years with extreme high and low
35 values in the time-series highlighted with filled circles. (d-i) Average seasonal
36 cycle (grey shading) and seasonal cycles during years with the extreme proxy
37 values detected in (a-c) shown with coloured lines for (d-f) Lillo precipitation
38 and (g-i) Lillo temperature. Where the coloured lines lie outside the grey
39 shading, significant deviations from average conditions occur. 9
- 40 6 Composites of wet summer conditions during years with extreme values in
41 the tree-ring series in the studied instrumental period (1925–2002). Note
42 that wet conditions correspond to wide (high) values in TRW and low values
43 for both stable isotopic ratios ($\delta^{13}\text{C}$ and $\delta^{18}\text{O}$). (a-l): Seasonal composite
44 anomalies for years with extreme proxy values are shown for those months
45 with significant deviations in the precipitation seasonal cycle (Fig. 5d-f) for (a-
46 c) precipitation, (d-f) surface air temperature (SAT), (g-i) moisture transport
47 integrated below 500hPa, and (j-l) Sea Level Pressure (SLP). Dashed contours
48 and black arrows indicate anomalies significant at the 90% confidence level. 11
- 49 7 Composites of dry summer conditions during years with extreme values in the
50 tree-ring series for the studied instrumental period (1925–2002). Note that
51 dry conditions correspond to narrow (low) values in TRW and high values
52 for both stable isotopic ratios ($\delta^{13}\text{C}$ and $\delta^{18}\text{O}$). (a-l): Seasonal composite
53 anomalies for years with extreme proxy values are shown for those months with
54 significant deviations in the precipitation seasonal cycle (Fig. 5d-f) for (a-c)
55 precipitation, (d-f) surface air temperature (SAT), (g-i) moisture transport
56 integrated below 500hPa, and (j-l) Sea Level Pressure (SLP). Dashed contours
57 and black arrows indicate anomalies significant at the 90% level. 13

58	8	Seasonal composite analyses of SLP (mb) during years with extreme values	
59		in the tree-ring series for the pre-instrumental period (1665-1900). Note that	
60		wet conditions over the Lillo site correspond to wide (high) values in TRW	
61		(a) and low values for both stable isotopic ratios $\delta^{13}\text{C}$ (b) and $\delta^{18}\text{O}$ (c); dry	
62		conditions to narrow (low) values in TRW (d) and high values for both stable	
63		isotopic ratios $\delta^{13}\text{C}$ (e) and $\delta^{18}\text{O}$ (f). n indicates the number of extreme years	
64		used in each composite that was based on the criteria to select years above	
65		and below the threshold established in Fig. 3.	14
66	9	As Fig. 8, but for the self-calibrating Palmer Drought Severity Index (scPDSI)	
67		from the Old World Drought Atlas.	15
68	10	As Fig. 8, but using the years detected by the 8 high / low proxy values	
69		for the instrumental period (1925–1999) for the SLP anomaly composites. n	
70		indicates the number of extreme years used in each composite. Note that 7	
71		years were used instead of 8 in some cases when the year 2001 needed to be	
72		excluded because it was not available in the SLP gridded product.	16
73	11	As Fig. 8, but using the years detected by the 8 high / low proxy values from	
74		the instrumental period (1925–2002) for the scPDSI anomaly composites.	17
75	12	Time-series of the number of extreme events in 20-yr sliding windows for the	
76		extreme values in both $\delta^{13}\text{C}$ and $\delta^{18}\text{O}$ records. Wet (dry) conditions are	
77		reflected by low (high) isotopic extreme values.	18

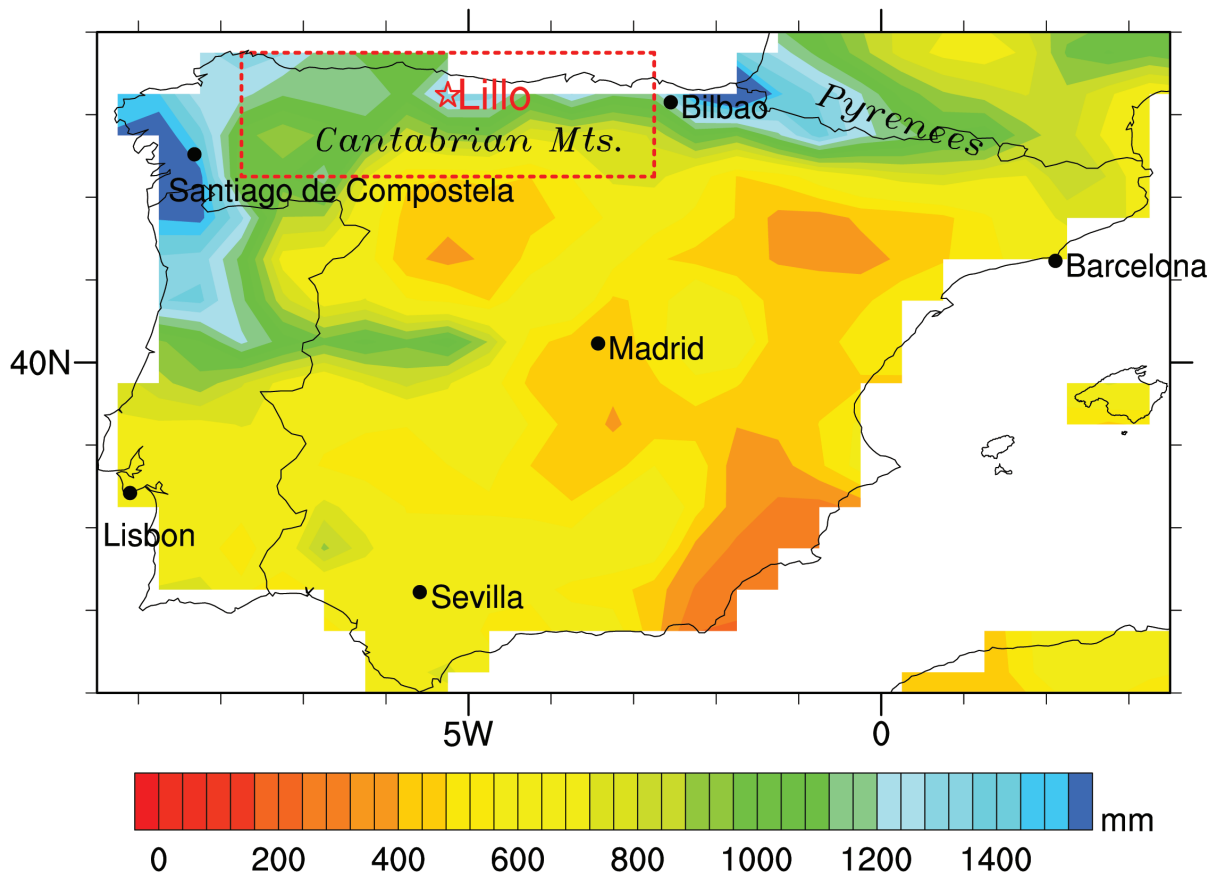


FIG. 1. Mean observed annual precipitation (mm) in the Iberian Peninsula for the period 1901–2002: The Lillo study site (star) and other key locations are indicated. Red dashed box delimits the target region used to create the Lillo precipitation and temperature time series used in this study.

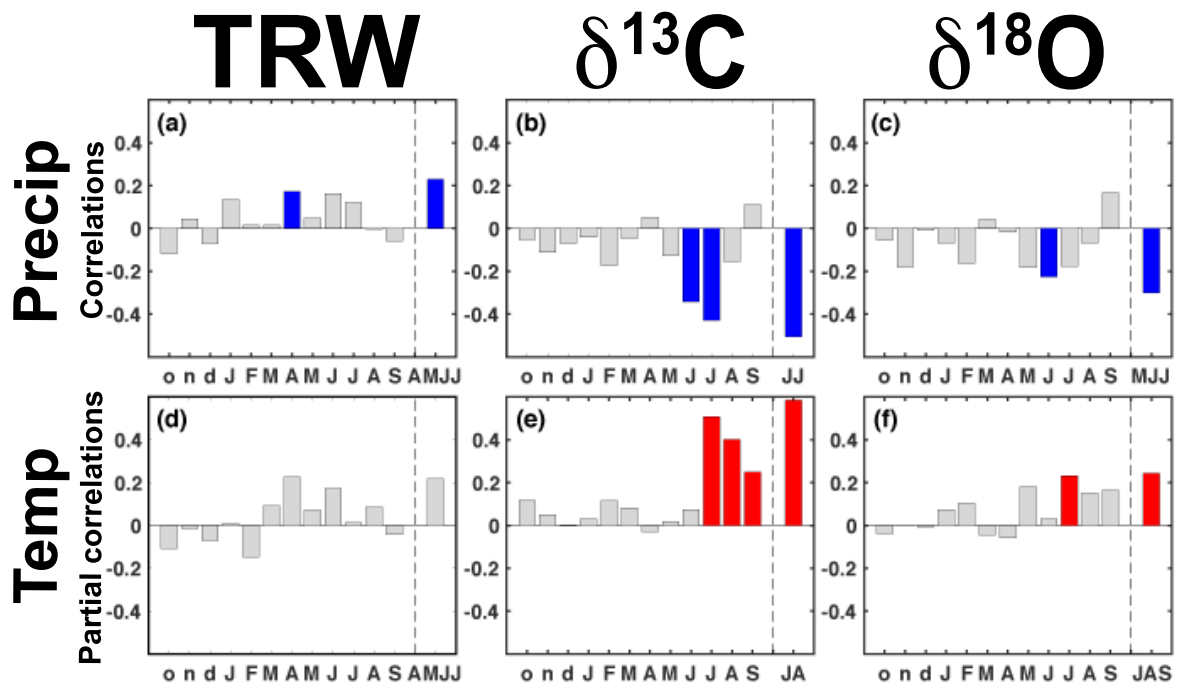


FIG. 2. Correlations for monthly precipitation and partial correlations for temperature, both from October in the previous year to September of the current year for the period 1925–2002 with tree-ring parameters for (left) TRW, (middle) $\delta^{13}\text{C}$, and (right) $\delta^{18}\text{O}$. Note that coloured bars indicate significant correlation coefficients at the 95% confidence level.

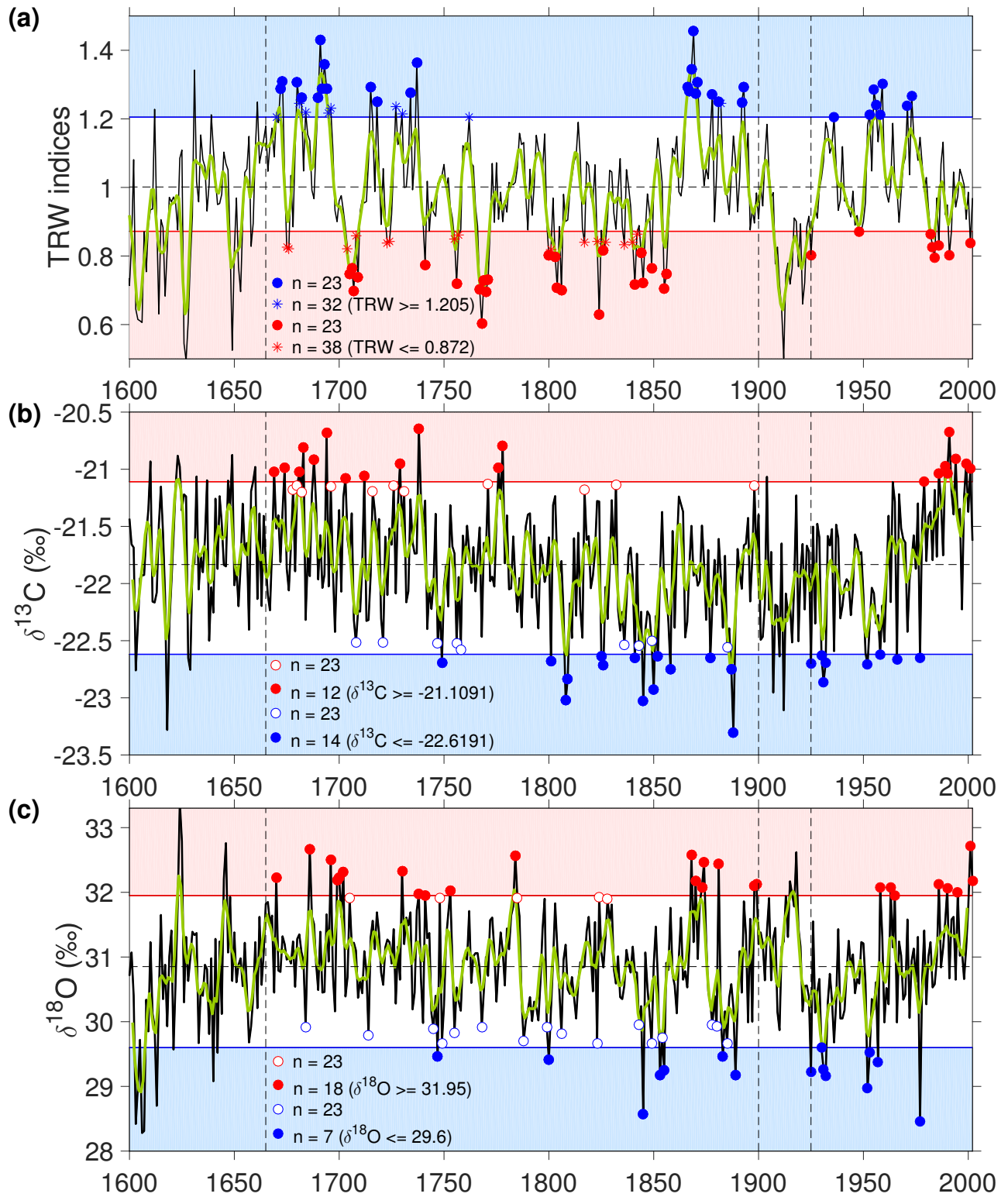


FIG. 3. Time-series of the Lillo tree-ring chronologies for the period 1600–2002 for (a) TRW, (b) $\delta^{13}\text{C}$, and (c) $\delta^{18}\text{O}$. The circles in the period from 1665 to 1900 show the years with extreme values in the top and bottom deciles of the proxy times-series: the 23 highest and 23 lowest values (Table 2). Filled circles indicate that the values are above or below the thresholds (horizontal lines) established in the instrumental period by the lowest of the uppermost decile and the highest of the lowermost decile of the proxy values in the analysis period 1925–2002 (Table 1). Dashed lines delineate the studied pre-instrumental period from 1665 to 1900 and the instrumental period from 1925 to 2002 used for the analyses shown in Figs. 5-7

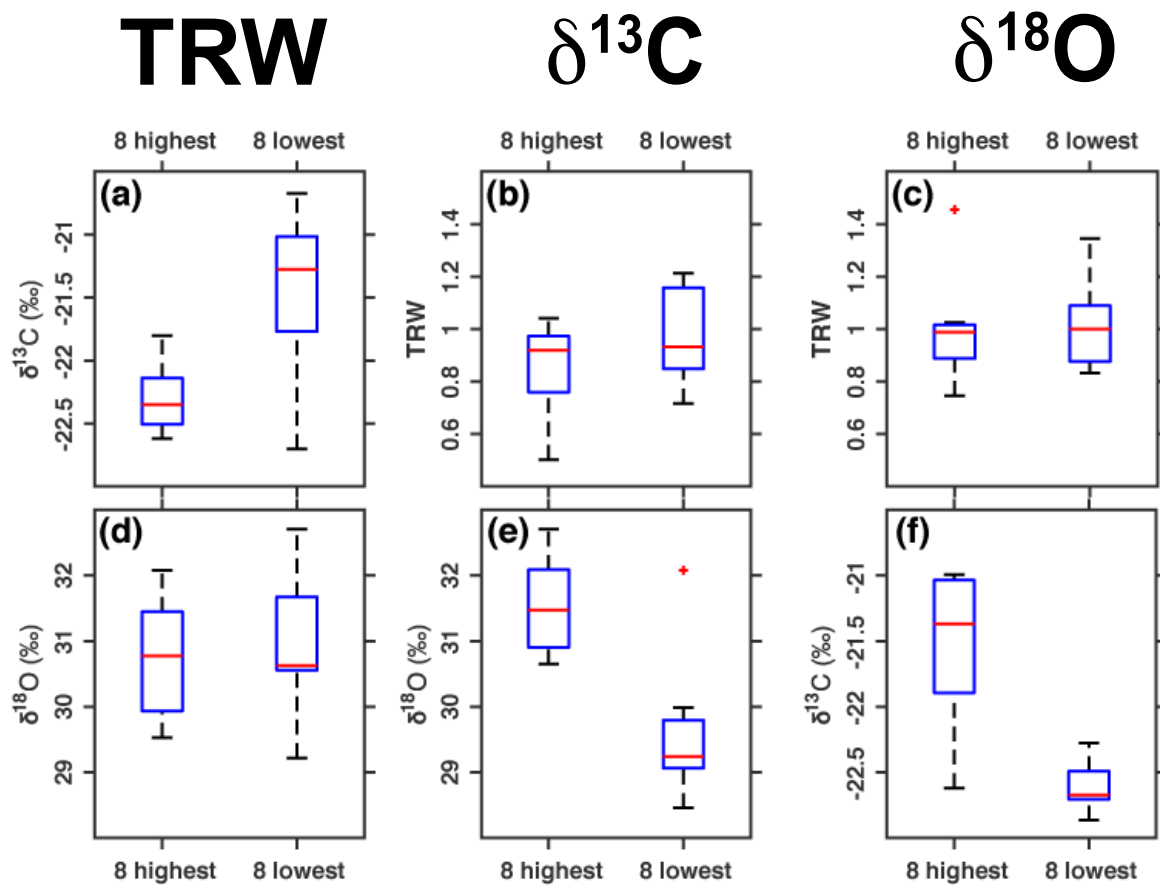


FIG. 4. Box-and-whisker plots for the values of the tree-ring records during the 8 years of extreme high/low values for each tree-ring records: (left) TRW, (middle) $\delta^{13}\text{C}$ and (right) $\delta^{18}\text{O}$. The red line represents the median, the blue boxes delimit the 25th and 75th percentile (i.e. interquartile range) and whiskers the minimum and maximum values.

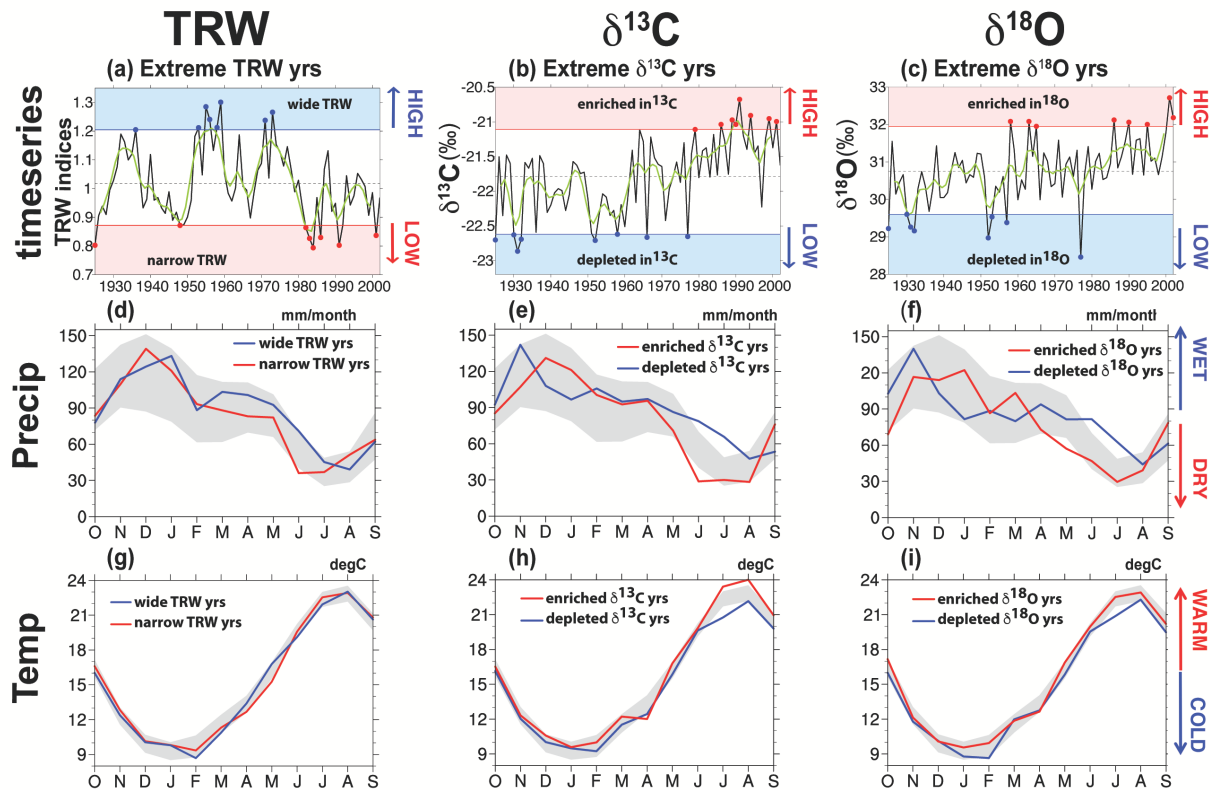


FIG. 5. Lillo tree-ring series and seasonal cycles for precipitation and temperature: (a-c) Time-series of the Lillo tree-ring chronologies for the period 1925–2002 for (left) TRW, (middle) $\delta^{13}\text{C}$, and (right) $\delta^{18}\text{O}$. Annual values are shown in black, 5-year moving average in green, and years with extreme high and low values in the time-series highlighted with filled circles. (d-i) Average seasonal cycle (grey shading) and seasonal cycles during years with the extreme proxy values detected in (a-c) shown with coloured lines for (d-f) Lillo precipitation and (g-i) Lillo temperature. Where the coloured lines lie outside the grey shading, significant deviations from average conditions occur.

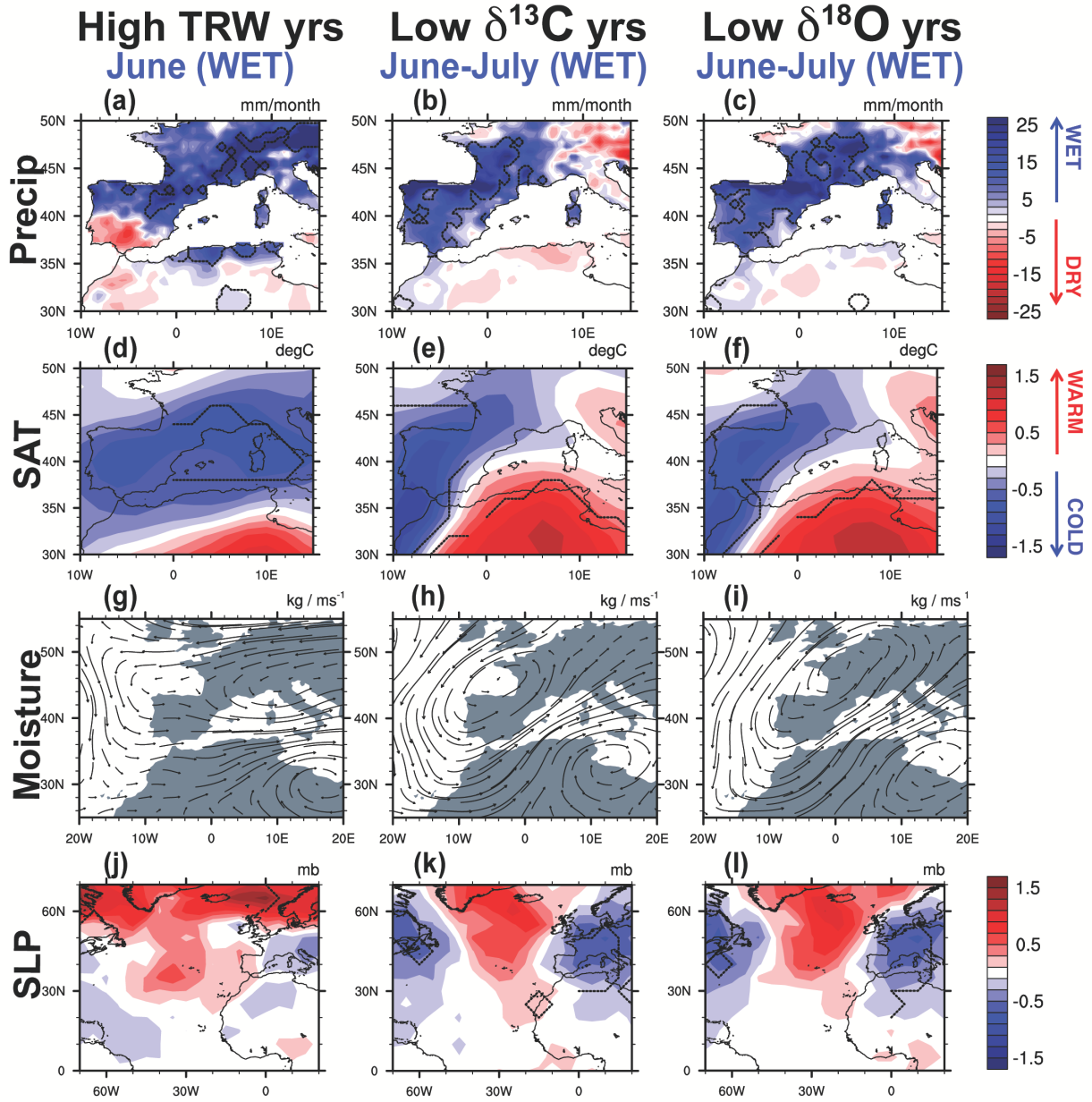


FIG. 6. Composites of wet summer conditions during years with extreme values in the tree-ring series in the studied instrumental period (1925–2002). Note that wet conditions correspond to wide (high) values in TRW and low values for both stable isotopic ratios ($\delta^{13}\text{C}$ and $\delta^{18}\text{O}$). (a-l): Seasonal composite anomalies for years with extreme proxy values are shown for those months with significant deviations in the precipitation seasonal cycle (Fig. 5d-f) for (a-c) precipitation, (d-f) surface air temperature (SAT), (g-i) moisture transport integrated below 500hPa, and (j-l) Sea Level Pressure (SLP). Dashed contours and black arrows indicate anomalies significant at the 90% confidence level.

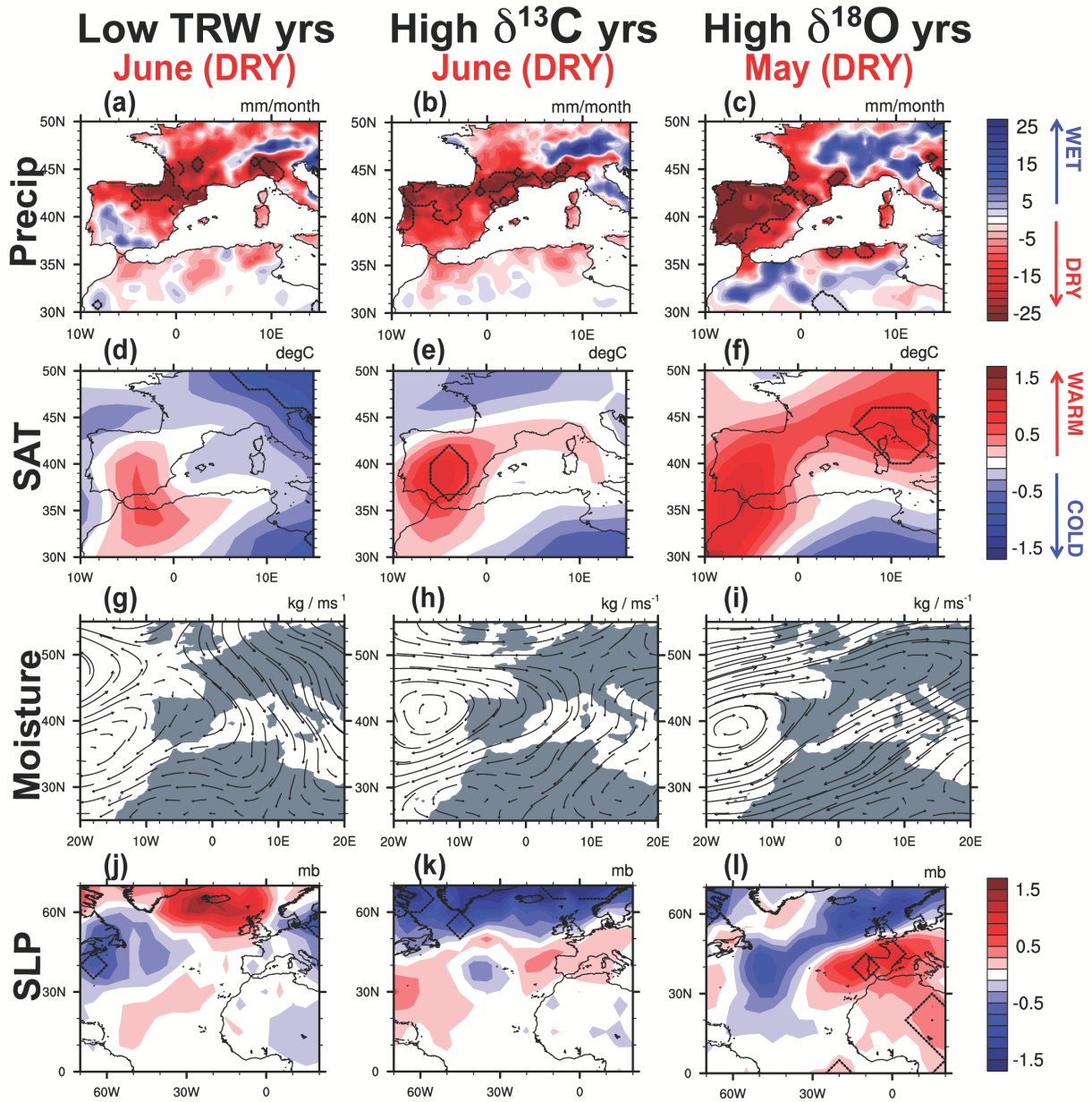


FIG. 7. Composites of dry summer conditions during years with extreme values in the tree-ring series for the studied instrumental period (1925–2002). Note that dry conditions correspond to narrow (low) values in TRW and high values for both stable isotopic ratios ($\delta^{13}\text{C}$ and $\delta^{18}\text{O}$). (a-l): Seasonal composite anomalies for years with extreme proxy values are shown for those months with significant deviations in the precipitation seasonal cycle (Fig. 5d-f) for (a-c) precipitation, (d-f) surface air temperature (SAT), (g-i) moisture transport integrated below 500hPa, and (j-l) Sea Level Pressure (SLP). Dashed contours and black arrows indicate anomalies significant at the 90% level.

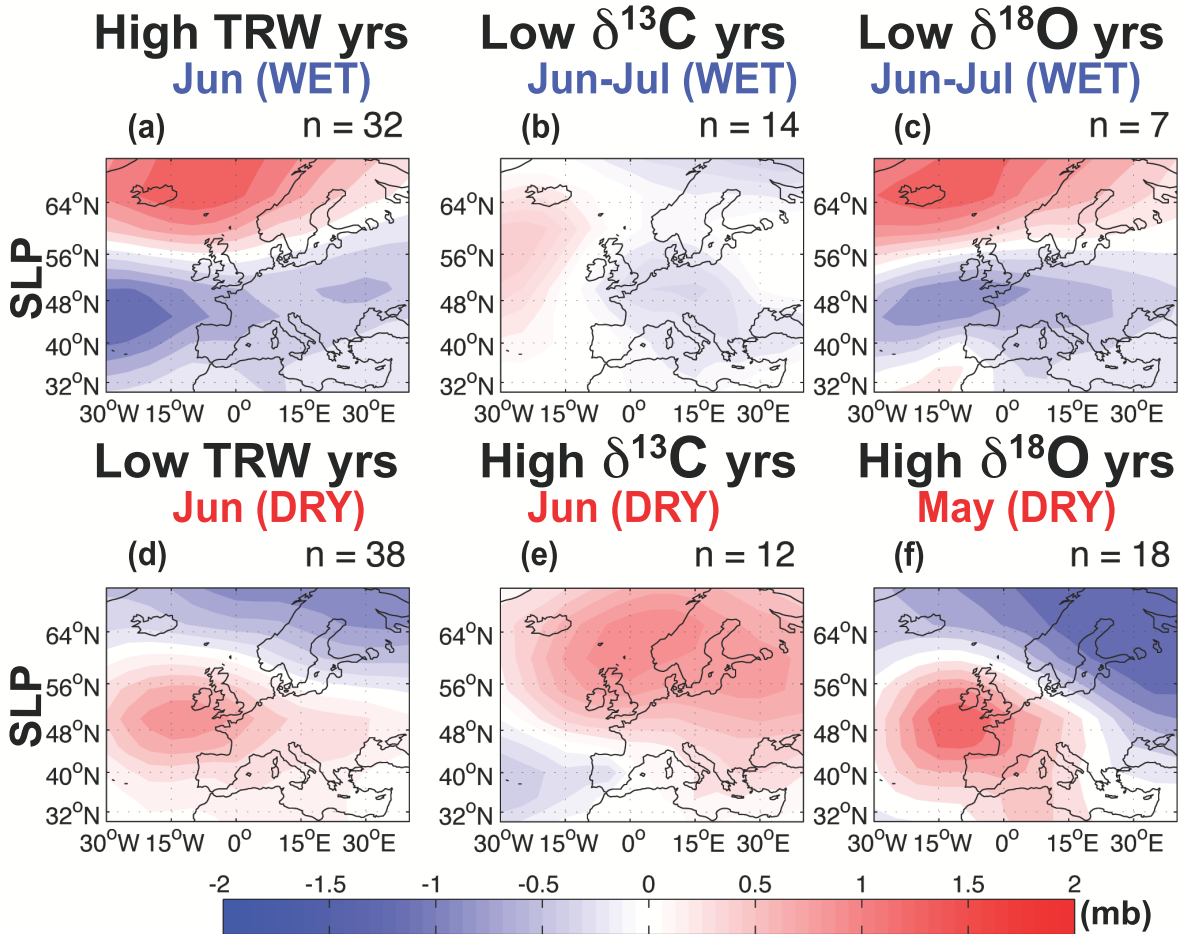


FIG. 8. Seasonal composite analyses of SLP (mb) during years with extreme values in the tree-ring series for the pre-instrumental period (1665-1900). Note that wet conditions over the Lillo site correspond to wide (high) values in TRW (a) and low values for both stable isotopic ratios $\delta^{13}\text{C}$ (b) and $\delta^{18}\text{O}$ (c); dry conditions to narrow (low) values in TRW (d) and high values for both stable isotopic ratios $\delta^{13}\text{C}$ (e) and $\delta^{18}\text{O}$ (f). n indicates the number of extreme years used in each composite that was based on the criteria to select years above and below the threshold established in Fig. 3.

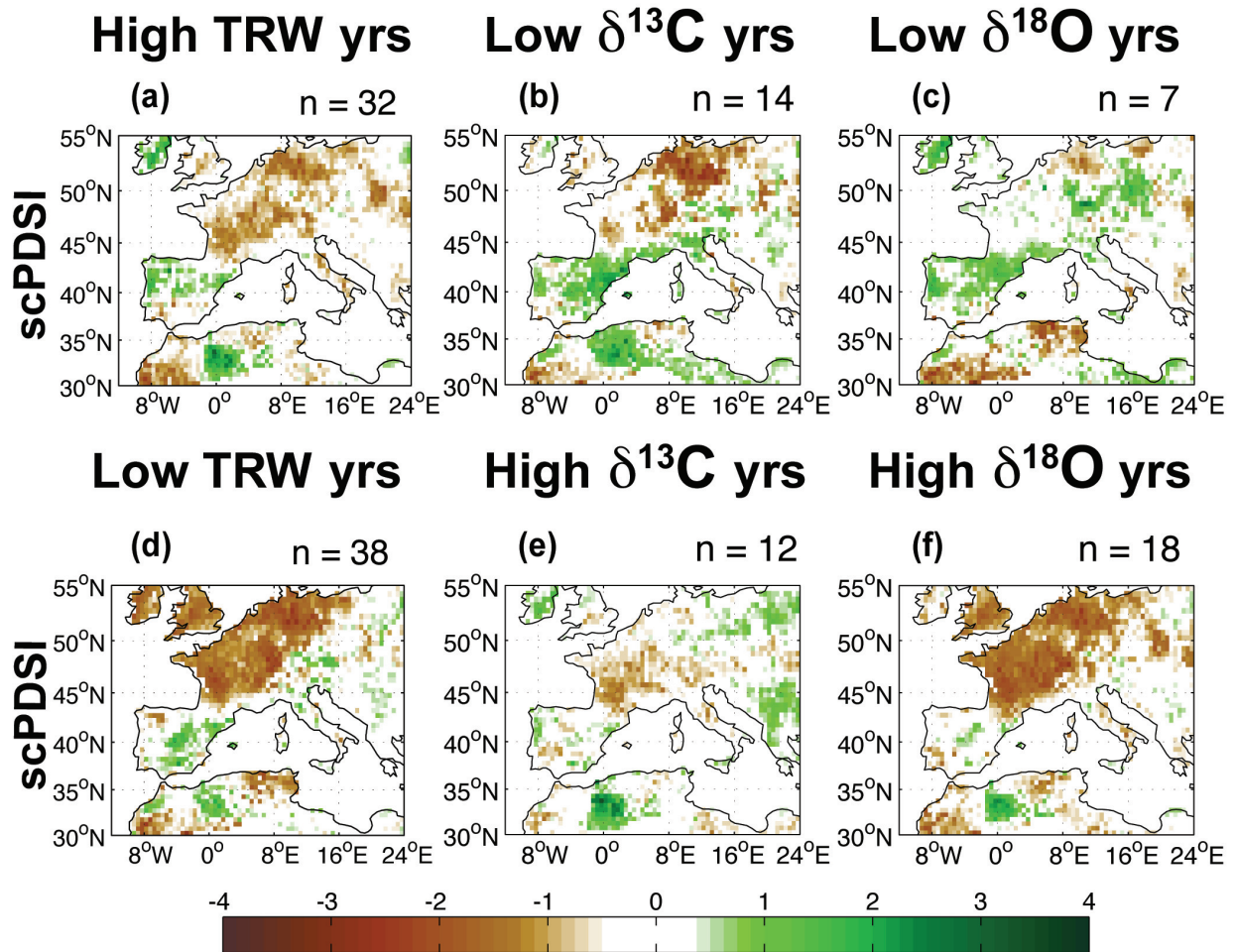


FIG. 9. As Fig. 8, but for the self-calibrating Palmer Drought Severity Index (scPDSI) from the Old World Drought Atlas.

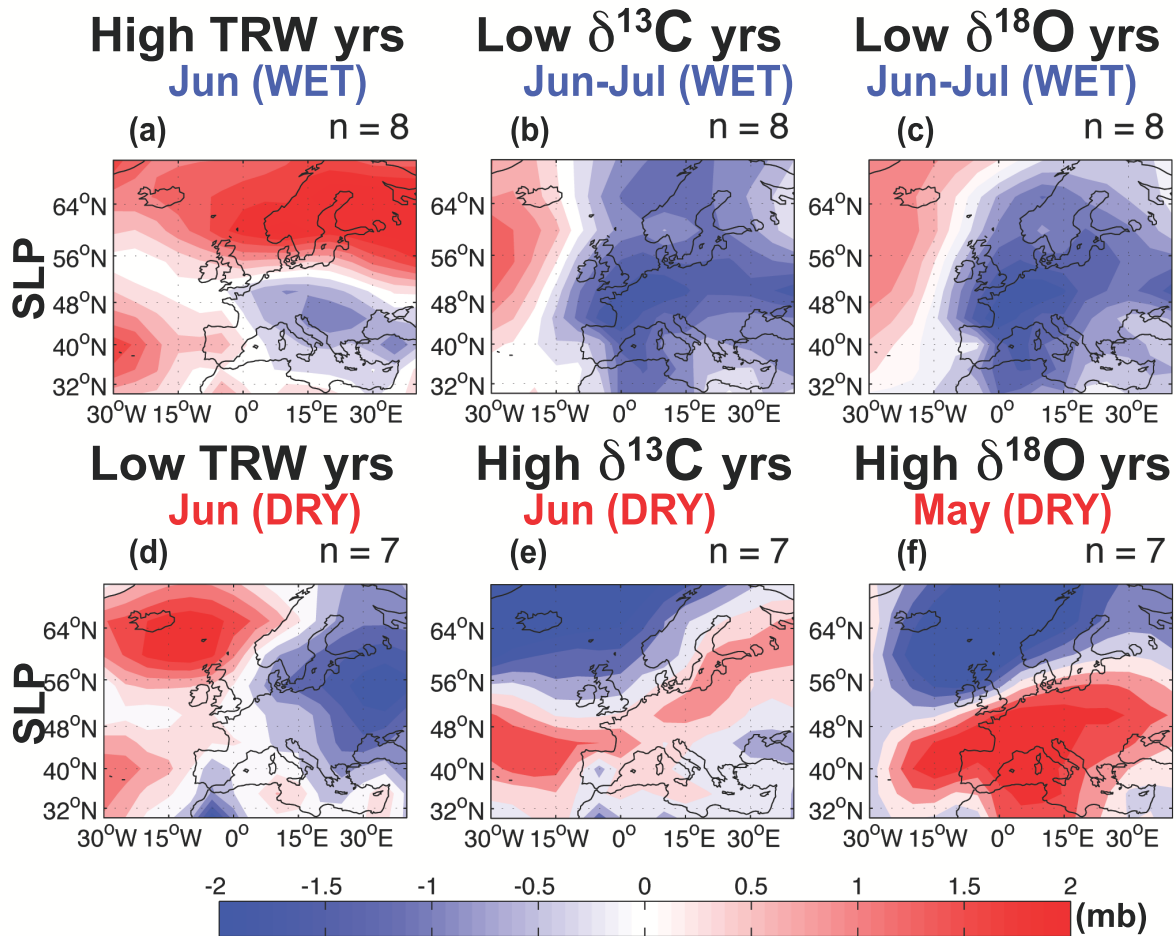


FIG. 10. As Fig. 8, but using the years detected by the 8 high / low proxy values for the instrumental period (1925–1999) for the SLP anomaly composites. n indicates the number of extreme years used in each composite. Note that 7 years were used instead of 8 in some cases when the year 2001 needed to be excluded because it was not available in the SLP gridded product.

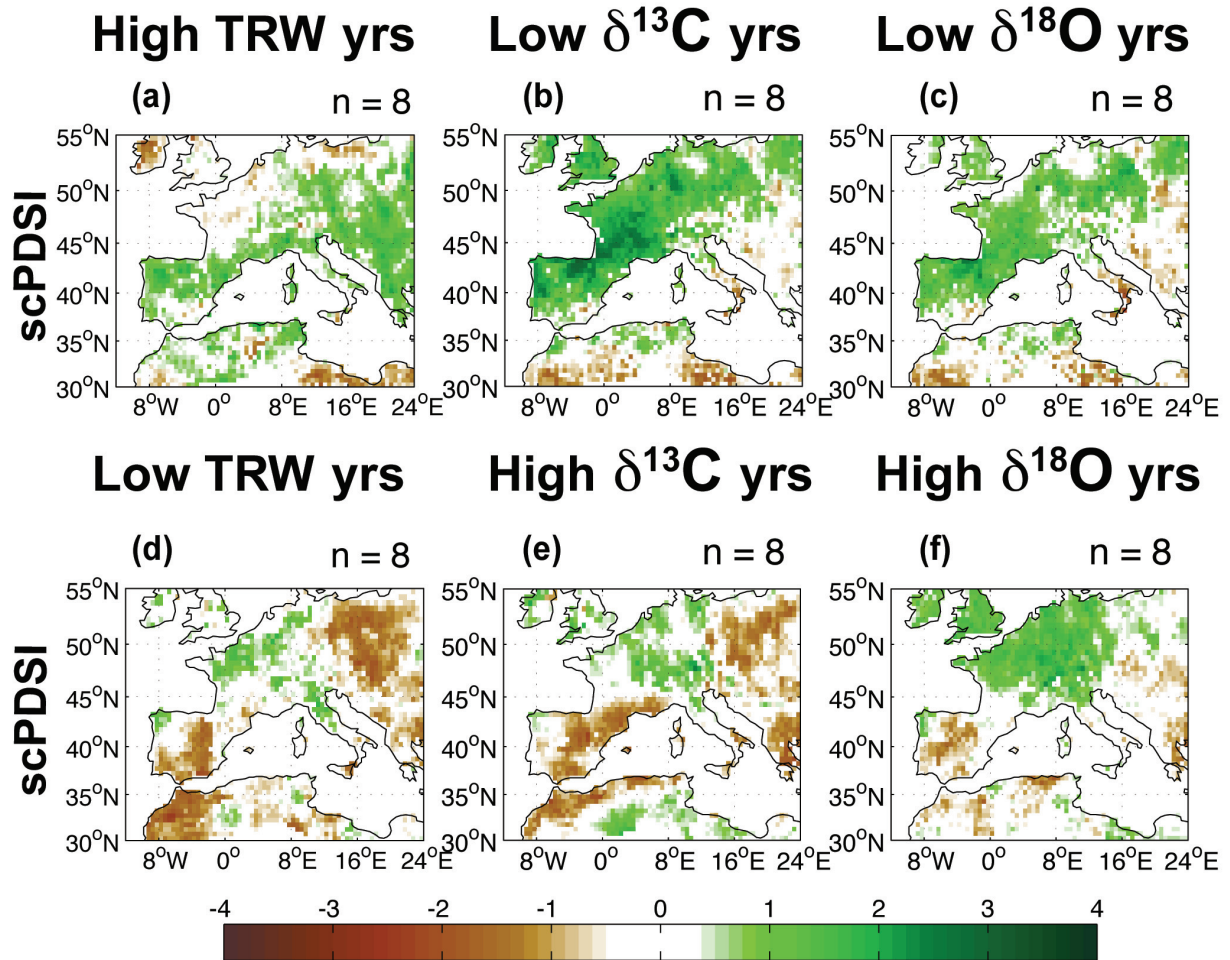


FIG. 11. As Fig. 8, but using the years detected by the 8 high / low proxy values from the instrumental period (1925–2002) for the scPDSI anomaly composites.

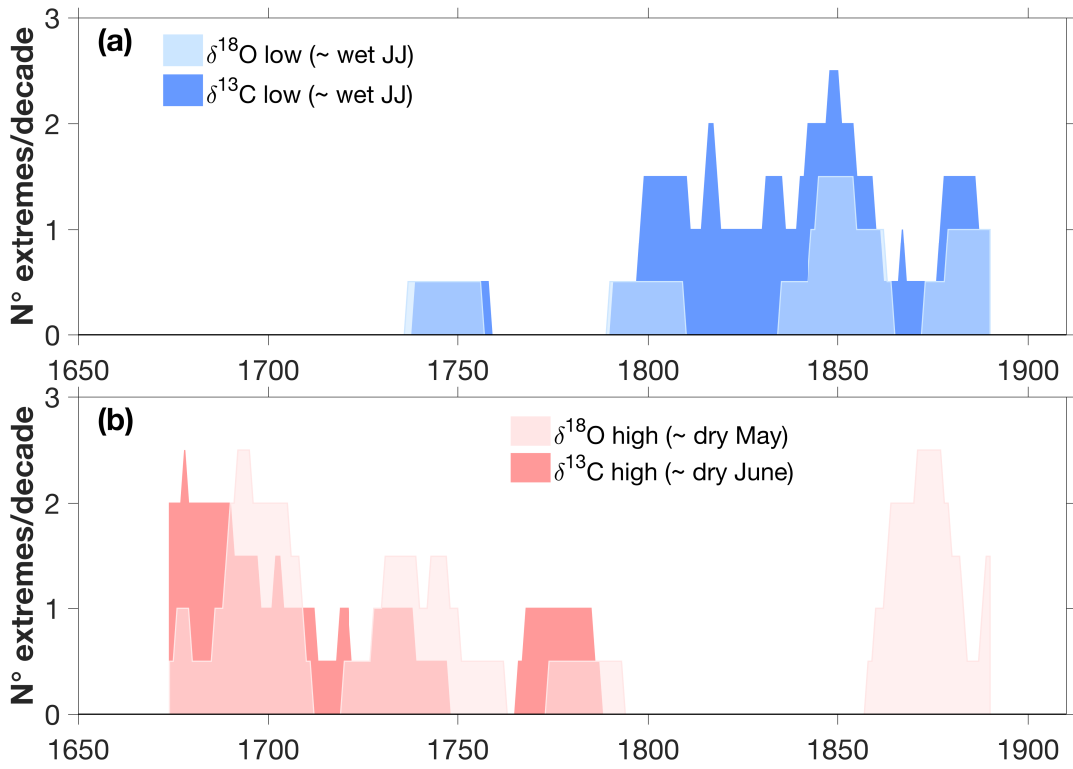


FIG. 12. Time-series of the number of extreme events in 20-yr sliding windows for the extreme values in both $\delta^{13}\text{C}$ and $\delta^{18}\text{O}$ records. Wet (dry) conditions are reflected by low (high) isotopic extreme values.